

Lightness of Higgs Boson and Spontaneous CP-violation in the Lee Model: An Alternative Scenario

Ying-nan Mao ^{1,4,*} and Shou-hua Zhu ^{1,2,3,†}

¹ *Institute of Theoretical Physics & State Key Laboratory of Nuclear Physics and Technology,
Peking University, Beijing 100871, China*

² *Collaborative Innovation Center of Quantum Matter, Beijing 100871, China*

³ *Center for High Energy Physics, Peking University, Beijing 100871, China*

⁴ *Center for Future High Energy Physics & Theoretical Physics Division,
Institute of High Energy Physics, Chinese Academy of Sciences, Beijing 100049, China*

(Dated: September 13, 2016)

Based on the weakly-coupled spontaneous CP-violation two-Higgs-doublet model (named Lee model) and the mechanism to generate the correlation between smallness of CP-violation and lightness of scalar mass, as we proposed earlier, we predicted a light CP-mixing scalar η in which pseudoscalar component is dominant. It is a natural scenario in which $m_\eta \sim \mathcal{O}(10\text{GeV}) \ll v$. It means new physics might be hidden below the electro-weak scale v . Masses of all other scalars (h, H, H^\pm) should be around the electro-weak scale v . Among them, the 125 GeV Higgs boson (h) couplings are standard-model like, and the charged Higgs boson (H^\pm) mass should be around the heaviest neutral scalar (H) mass. We discussed all experimental constraints and showed that this scenario is still allowed by data. The strictest constraints come from the flavor violation experiments and the EDM of electron and neutron. We also discussed the future tests for this scenario. It is possible to discover the extra scalars or exclude this scenario at future colliders, especially at the LHC and e^+e^- colliders with $\mathcal{O}(\text{ab}^{-1})$ luminosity. We also pointed out that the Z -mediated Higgs pair production via $e^+e^- \rightarrow h_i h_j$ (h_i, h_j stand for two of the η, h, H) would be the key observable to confirm or exclude CP-violation in Higgs sector. The sensitivity to test this scenario is worth further studying in detail.

* maoyingnan@pku.edu.cn, maoyin@ihep.ac.cn

† shzhu@pku.edu.cn

I. INTRODUCTION

The realization of electro-weak symmetry breaking and CP-violation are two important topics both in the standard model (SM) and beyond the standard model (BSM). It is also attractive to relate them with each other. In our previous work [1], we proposed the correlation between lightness of Higgs boson and smallness of CP-violation. In this paper, we will continue to explore an alternative natural scenario and its phenomenology.

In 1964, the Higgs mechanism [2] was proposed. In the Higgs mechanism, a scalar doublet with nontrivial vacuum expectation value (VEV) was introduced to break the electro-weak gauge symmetry spontaneously. After spontaneous gauge symmetry breaking in the SM, there exists a scalar named the Higgs boson ¹. In July 2012, both ATLAS [4] and CMS [5] collaborations at LHC discovered a new boson with its mass around 125 GeV [6]. The subsequent measurements by CMS and ATLAS [7–9] on its signal strengths showed that the scalar behaves similarly with SM Higgs boson. However there is still spacious room for the BSM. In some BSM models, there exist new light particles which may appear in the final states during Higgs decay processes. For example, in the next-to-minimal supersymmetric standard model (NMSSM) [10], the simplest little Higgs model (SLH) [11–13], or the left-right-twin-Higgs model (LRTH) [14, 15], a light scalar η with its mass of $\mathcal{O}(10)\text{GeV}$ will naturally appear. For some cases in 2HDM [16–20], a light scalar η is allowed as well, though there are strict constraints on them. If $m_\eta < m_h/2 = 62.5\text{GeV}$, there would be an exotic decay channel $h \rightarrow \eta\eta$; while if $m_\eta < m_h - m_Z = 34\text{GeV}$, an exotic decay channel $h \rightarrow Z\eta$ should also be open. There is no evidence for exotic Higgs decay channels at LHC till now, the constraints on the exotic Higgs decay branching ratio is set to be $\text{Br}_{\text{exo}} \lesssim (20-30)\%$ [21] if the production rate of the Higgs boson is close to that in SM. The spin-parity property for Higgs boson is expected to be 0^+ in the SM. Experimentally, a pure pseudoscalar state (0^-) is excluded at over 3σ [22–24]. But a mixing state is still allowed, thus the spacious room for BSM scenarios have not been closed yet.

Theoretically, CP-violation in SM is induced by the Kobayashi and Maskawa (K-M) mechanism [25] proposed by Kobayashi and Maskawa in 1973. They proved that a nontrivial

¹ There may exist more particles in the extension of SM. For example, in the two-Higgs-doublet model (2HDM) [3] in which two scalar doublets were introduced, there exist five scalars. Two of them are charged and three of them are neutral.

phase which leads to CP-violation in quark mixing matrix (called the CKM matrix [25, 26]) would appear if there exist three or more generations of quarks. The CKM matrix is usually parameterized as the Wolfenstein formalism [27]

$$V_{\text{CKM}} = \begin{pmatrix} 1 - \lambda^2/2 & \lambda & A\lambda^3(\rho - i\eta) \\ -\lambda & 1 - \lambda^2/2 & A\lambda^2 \\ A\lambda^3(1 - \rho - i\eta) & -A\lambda^2 & 1 \end{pmatrix} + \mathcal{O}(\lambda^4). \quad (1)$$

The Jarlskog invariant J [28] defined as

$$\det \left(i \left[M_U M_U^\dagger, M_D M_D^\dagger \right] \right) = 2J \prod_{i < j} (m_{U_i}^2 - m_{U_j}^2) \prod_{i < j} (m_{D_i}^2 - m_{D_j}^2) \quad (2)$$

measures the effects of CP-violation where $M_{U(D)}$ is the mass matrix for up (down) type quarks. $J \approx \lambda^6 A^2 \eta \approx 3 \times 10^{-5}$ [29] means CP-violation in SM is small. Experimentally, in K- and B-meson systems, several kinds of CP-violation have been discovered [29] which represent the success of K-M mechanism. While it is still attractive to search for new sources of CP-violation, not only to search for BSM physics, but also to understand the matter-antimatter asymmetry in the universe [29, 30]. SM itself cannot provide enough baryogenesis effects [29–32], but in some extensions of SM, for example, 2HDM with CP-violation in Higgs sector, it is possible to generate large enough baryogenesis effect [31, 33].

Lee model [34] is a possible way to connect Higgs mechanism and CP-violation with each other. It was proposed by Lee in 1973 as the first 2HDM. In Lee model, the lagrangian is required to be CP-conserved, but the VEV of one Higgs doublet can be complex, thus the CP symmetry is spontaneously broken due to the complex vacuum. In this case, the neutral scalars are CP-mixing states so that CP-violation effects should occur in the Higgs sector. All the three neutral scalars should couple to massive gauge bosons with the effective interaction

$$\mathcal{L}_{h_i VV} = \sum_i c_{i,V} h_i \left(\frac{2m_W^2}{v} W^{+\mu} W_\mu^- + \frac{m_Z^2}{v} Z^\mu Z_\mu \right) \quad (3)$$

where $c_{i,V} \equiv g_{h_i VV} / g_{hV V, \text{SM}}$ is the ratio between the $h_i VV$ coupling strength and that in SM. $c_{1,V}^2 + c_{2,V}^2 + c_{3,V}^2 = 1$ due to the mechanism of spontaneous gauge symmetry breaking. The quantity

$$K \equiv c_{1,V} c_{2,V} c_{3,V} \quad (4)$$

measures the CP-violation effects in Higgs sector [3, 35] when the masses of the neutral

scalars are non-degenerate ². In our recent paper [1], we proposed the correlation between lightness of Higgs boson and smallness of CP-violation through small $t_\beta s_\xi$ in Lee model ³. While in that paper, we treated the 125 GeV scalar as the lightest one thus it implied a strong-interacted scenario beyond [36]. However, another natural scenario with a weakly-interacted scalar in which the heavy scalars have the mass $m_i \sim \mathcal{O}(v)$ is also possible where $v = 246\text{GeV}$ is the VEV of the scalar doublet in SM. In this scenario, Lee model would predict a light scalar η with mass $m_\eta \ll v$ for the small $t_\beta s_\xi$ case based on our paper [1]. In this paper, we will discuss this scenario and its phenomenology.

This paper is organized as follows. In section II we introduce the Lee model and its main properties. In section III we discuss the constraints for this scenario by recent experiments, including data from both high and low energy phenomena. In section IV we consider the predictions and future tests for this scenario. And section V contains our conclusions and discussions.

II. THE LEE MODEL AND A LIGHT SCALAR

In Lee model [34], the lagrangian is required to be CP-conserved in both scalar and Yukawa sectors. For the scalar sector,

$$\mathcal{L} = (D_\mu \phi_1)^\dagger (D^\mu \phi_1) + (D_\mu \phi_2)^\dagger (D^\mu \phi_2) - V(\phi_1, \phi_2) \quad (5)$$

in which the scalar potential

$$\begin{aligned} V(\phi_1, \phi_2) = & \mu_1^2 R_{11} + \mu_2^2 R_{22} + \lambda_1 R_{11}^2 + \lambda_2 R_{11} R_{12} \\ & + \lambda_3 R_{11} R_{22} + \lambda_4 R_{12}^2 + \lambda_5 R_{12} R_{22} + \lambda_6 R_{22}^2 + \lambda_7 I_{12}^2. \end{aligned} \quad (6)$$

Here the scalar doublets

$$\phi_1 = \begin{pmatrix} \phi_1^+ \\ \frac{v_1 + R_1 + iI_1}{\sqrt{2}} \end{pmatrix}, \quad \phi_2 = \begin{pmatrix} \phi_2^+ \\ \frac{v_2 e^{i\xi} + R_2 + iI_2}{\sqrt{2}} \end{pmatrix} \quad (7)$$

² If at least two of the scalars have the same mass, we can always perform a field rotation between them to keep at least one $c_{i,V} = 0$, thus there would be no CP-violation in Higgs sector.

³ The parameters will be defined next section, or see [1].

and $R(I)_{ij}$ denotes the real (imaginary) part of $\phi_i^\dagger \phi_j$ ⁴. $\sqrt{v_1^2 + v_2^2} = v = 246\text{GeV}$. The general Yukawa couplings can be written as

$$\mathcal{L}_y = -\bar{Q}_{Li}((Y_{1d})_{ij}\phi_1 + (Y_{2d})_{ij}\phi_2)D_{Rj} - \bar{Q}_{Li}((Y_{1u})_{ij}\tilde{\phi}_1 + (Y_{2u})_{ij}\tilde{\phi}_2)U_{Rj}, \quad (8)$$

where all coupling constants should be real and $\tilde{\phi}_i \equiv i\sigma_2\phi_i^*$. We choose the Type III [3, 37] Yukawa couplings because there is no additional discrete symmetry to forbid any term in (8). It is possible to generate correct fermion mass spectrum and CKM matrix from (8), for example, see [38, 39].

We should minimize the potential (6). For some parameter choices, there is a nonzero ξ which means the spontaneous CP- violation ⁵. If $v_1, v_2, \xi \neq 0$, we have

$$\mu_1^2 = -\lambda_1 v_1^2 - \frac{\lambda_3 + \lambda_7}{2} v_2^2 - \frac{\lambda_2}{2} v_1 v_2 \cos \xi; \quad (9)$$

$$\mu_2^2 = -\frac{\lambda_3 + \lambda_7}{2} v_1^2 - \lambda_6 v_2^2 - \frac{\lambda_5}{2} v_1 v_2 \cos \xi; \quad (10)$$

$$0 = \frac{\lambda_2}{2} v_1^2 + \frac{\lambda_5}{2} v_2^2 + (\lambda_4 - \lambda_7) v_1 v_2 \cos \xi. \quad (11)$$

$|\lambda_2 v_1^2 + \lambda_5 v_2^2| < 2|\lambda_4 - \lambda_7| v_1 v_2$ is required to keep $\xi \neq 0$. Define $s_\alpha \equiv \sin \alpha, c_\alpha \equiv \cos \alpha, t_\alpha \equiv \tan \alpha$ in the following parts of this paper, and $t_\beta \equiv v_2/v_1$ is the ratio of the VEVs for scalar doublets. The vacuum stability conditions can be found in [3] or Appendix. A in [1]. The Goldstone fields can be written as

$$G^\pm = c_\beta \phi_1^\pm + e^{\mp i\xi} s_\beta \phi_2^\pm; \quad (12)$$

$$G^0 = c_\beta I_1 + s_\beta c_\xi I_2 - s_\beta s_\xi R_2. \quad (13)$$

The charged Higgs field is orthogonal to the corresponding charged Goldstone field as

$$H^\pm = -e^{\pm i\xi} s_\beta \phi_1^\pm + c_\beta \phi_2^\pm \quad (14)$$

with the mass square

$$m_\pm^2 = -\frac{\lambda_7}{2} v^2. \quad (15)$$

⁴ We can always perform a rotation between ϕ_1 and ϕ_2 to keep the term proportional to R_{12} vanish.

⁵ We can always perform a global phase redefinition for ϕ_1 and ϕ_2 to keep one of the VEVs real, just like the case in (7).

The symmetric mass matrix \tilde{m} for neutral scalars is written as [1]

$$\begin{pmatrix} (\lambda_4 - \lambda_7)s_\xi^2 & -((\lambda_4 - \lambda_7)s_\beta c_\xi + \lambda_2 c_\beta)s_\xi & -((\lambda_4 - \lambda_7)c_\beta c_\xi + \lambda_5 s_\beta)s_\xi \\ & 4\lambda_1 c_\beta^2 + \lambda_2 s_{2\beta} c_\xi + (\lambda_4 - \lambda_7)s_\beta^2 c_\xi^2 & ((\lambda_3 + \lambda_7) + (\lambda_4 - \lambda_7)c_\xi^2/2)s_{2\beta} \\ & & + \lambda_2 c_\beta^2 c_\xi + \lambda_5 s_\beta^2 c_\xi \\ & & (\lambda_4 - \lambda_7)c_\beta^2 c_\xi^2 \\ & & + \lambda_5 s_{2\beta} c_\xi + 4\lambda_6 s_\beta^2 \end{pmatrix} \quad (16)$$

in the basis $(-s_\beta I_1 + c_\beta c_\xi I_2 - c_\beta s_\xi R_2, R_1, s_\xi I_2 + c_\xi R_2)^T$ in unit of $v^2/2$. To solve the eigenvalue equation with perturbation method ⁶, we should expand \tilde{m} in powers of $(t_\beta s_\xi)$ in small t_β limit as

$$\tilde{m} = \tilde{m}_0 + (t_\beta s_\xi)\tilde{m}_1 + (t_\beta s_\xi)^2\tilde{m}_2 + \dots \quad (17)$$

For the two heavy scalars, we have [1]

$$m_{h,H}^2 = \frac{v^2}{2} \left((\tilde{m}_0)_{22(33)} + \mathcal{O}(t_\beta s_\xi) \right) \quad (18)$$

where

$$(\tilde{m}_0)_{22(33)} = \frac{4\lambda_1 + \lambda_4 - \lambda_7}{2} \mp \left(\frac{4\lambda_1 - (\lambda_4 - \lambda_7)}{2} c_{2\theta} + \lambda_2 s_{2\theta} \right). \quad (19)$$

Here $\theta = (1/2) \arctan(2\lambda_2/(4\lambda_1 - \lambda_4 + \lambda_7))$ labels the mixing angle of the real parts of the two scalar doublets. The scalar fields

$$\begin{pmatrix} h \\ H \end{pmatrix} = \begin{pmatrix} c_\theta & s_\theta \\ -s_\theta & c_\theta \end{pmatrix} \begin{pmatrix} R_1 \\ R_2 \end{pmatrix} + \mathcal{O}(t_\beta s_\xi). \quad (20)$$

We treat the lighter one as $m_h = \sqrt{(\tilde{m}_0)_{22}/2}v = 125\text{GeV}$. Different from the scenario in [1], in this paper, the dominant component for the 125 GeV scalar should be CP-even thus there exists SM limit for its couplings. While for the lightest scalar η , to the leading order

⁶ For the calculations in details, please see the Appendix.B in our recent paper [1], with the same conventions as those in this paper.

of $(t_\beta s_\xi)$, we have

$$\begin{aligned} m_\eta^2 &= \frac{v^2 t_\beta^2 s_\xi^2}{2} \left((\tilde{m}_2)_{11} - \frac{(\tilde{m}_1)_{12}^2}{(\tilde{m}_0)_{22}} - \frac{(\tilde{m}_1)_{13}^2}{(\tilde{m}_0)_{33}} \right) \\ &= \frac{v^2 t_\beta^2 s_\xi^2}{2} \left[4\lambda_6 + 2\lambda_5(\lambda_3 + \lambda_7)s_{2\theta} \left(\frac{1}{(\tilde{m}_0)_{22}} - \frac{1}{(\tilde{m}_0)_{33}} \right) \right. \\ &\quad \left. - 4(\lambda_3 + \lambda_7)^2 \left(\frac{c_\theta^2}{(\tilde{m}_0)_{22}} + \frac{s_\theta^2}{(\tilde{m}_0)_{33}} \right) - \lambda_5^2 \left(\frac{s_\theta^2}{(\tilde{m}_0)_{22}} + \frac{c_\theta^2}{(\tilde{m}_0)_{33}} \right) \right]; \end{aligned} \quad (21)$$

$$\begin{aligned} \eta &= I_2 - t_\beta s_\xi \left(\frac{(\tilde{m}_1)_{12}}{(\tilde{m}_0)_{22}} (c_\theta R_1 + s_\theta R_2) + \frac{(\tilde{m}_1)_{13}}{(\tilde{m}_0)_{33}} (c_\theta R_2 - s_\theta R_1) + \frac{I_1}{t_\xi} \right) \\ &= I_2 - t_\beta s_\xi \left[\left(2(\lambda_3 + \lambda_7) \left(\frac{c_\theta^2}{(\tilde{m}_0)_{22}} + \frac{s_\theta^2}{(\tilde{m}_0)_{33}} \right) + \frac{\lambda_5 s_{2\theta}}{2} \left(\frac{1}{(\tilde{m}_0)_{22}} - \frac{1}{(\tilde{m}_0)_{33}} \right) \right) R_1 \right. \\ &\quad \left. + \left((\lambda_3 + \lambda_7)s_{2\theta} \left(\frac{1}{(\tilde{m}_0)_{22}} - \frac{1}{(\tilde{m}_0)_{33}} \right) + \lambda_5 \left(\frac{s_\theta^2}{(\tilde{m}_0)_{22}} + \frac{c_\theta^2}{(\tilde{m}_0)_{33}} \right) \right) R_2 + \frac{I_1}{t_\xi} \right]. \end{aligned} \quad (22)$$

Thus in the limit $t_\beta s_\xi \rightarrow 0$, we have $m_\eta \propto t_\beta s_\xi \rightarrow 0$ and $\eta \rightarrow I_2$, which mean that η behaves like a light pseudoscalar but it has small CP-even component.

We can diagonalize the fermion mass matrixes as

$$V_{U,L} M_U V_{U,R}^\dagger = \begin{pmatrix} m_u & 0 & 0 \\ 0 & m_c & 0 \\ 0 & 0 & m_t \end{pmatrix}, \quad V_{D,L} M_D V_{D,R}^\dagger = \begin{pmatrix} m_d & 0 & 0 \\ 0 & m_s & 0 \\ 0 & 0 & m_b \end{pmatrix} \quad (23)$$

in which according to (8), the mass matrixes are

$$(M_U)_{ij} = \frac{v}{\sqrt{2}} ((Y_{1u})_{ij} c_\beta + (Y_{2u})_{ij} s_\beta e^{-i\xi}), \quad (M_D)_{ij} = \frac{v}{\sqrt{2}} ((Y_{1d})_{ij} c_\beta + (Y_{2d})_{ij} s_\beta e^{i\xi}). \quad (24)$$

The CKM matrix $V_{\text{CKM}} = V_{U,L} V_{D,L}^\dagger$ as usual. We can rewrite the Yukawa couplings (8) in quark sector as following adopting the Cheng-Sher ansatz [40]

$$\begin{aligned} \mathcal{L}'_{\text{Yuk,Q}} &= - \sum_{f=U_i, D_i} m_f \bar{f}_L f_R \left(1 + \frac{c_\beta R_1 + s_\beta c_\xi R_2 + s_\beta s_\xi I_2}{v} \right) \\ &\quad - \sum_{i,j} \frac{\xi_{ij}^U \sqrt{m_i^U m_j^U}}{v} \bar{U}_{i,L} U_{j,R} ((c_\beta R_2 - s_\beta c_\xi R_1 + s_\beta s_\xi I_1) - i(c_\beta I_2 - s_\beta c_\xi I_1 - s_\beta s_\xi R_1)) \\ &\quad - \sum_{i,j} \frac{\xi_{ij}^D \sqrt{m_i^D m_j^D}}{v} \bar{D}_{i,L} D_{j,R} ((c_\beta R_2 - s_\beta c_\xi R_1 + s_\beta s_\xi I_1) + i(c_\beta I_2 - s_\beta c_\xi I_1 - s_\beta s_\xi R_1)) \\ &\quad - \sum_{i,j} \frac{\sqrt{2m_i^D m_j^D}}{v} \bar{U}_{i,L} (V_{\text{CKM}} \cdot \xi^D)_{ij} D_{j,R} H^+ \\ &\quad - \sum_{i,j} \frac{\sqrt{2m_i^U m_j^U}}{v} \bar{D}_{i,L} (V_{\text{CKM}}^\dagger \cdot \xi^U)_{ij} U_{j,R} H^- + \text{h.c.} \end{aligned} \quad (25)$$

Similarly in the lepton sector

$$\begin{aligned}
\mathcal{L}'_{\text{Yuk},\ell} = & - \sum_{\ell} m_{\ell} \bar{\ell}_L \ell_R \left(1 + \frac{c_{\beta} R_1 + s_{\beta} c_{\xi} R_2 + s_{\beta} s_{\xi} I_2}{v} \right) \\
& - \sum_{i,j} \frac{\xi_{ij}^{\ell} \sqrt{m_i^{\ell} m_j^{\ell}}}{v} \bar{\ell}_{i,L} \ell_{j,R} ((c_{\beta} R_2 - s_{\beta} c_{\xi} R_1 + s_{\beta} s_{\xi} I_1) + i(c_{\beta} I_2 - s_{\beta} c_{\xi} I_1 - s_{\beta} s_{\xi} R_1)) \\
& - \sum_{i,j} \frac{\sqrt{2m_i^{\ell} m_j^{\ell}}}{v} \bar{\nu}_{i,L} (V_{\text{PMNS}} \cdot \xi^{\ell})_{ij} \ell_{j,R} H^+ + \text{h.c.}
\end{aligned} \tag{26}$$

Here V_{PMNS} is the lepton mixing matrix [41] and

$$\xi_{ij}^U = (V_{U,L})_{ik} (-s_{\beta} e^{i\xi} (Y_{1u})_{kl} + c_{\beta} (Y_{2u})_{kl}) (V_{U,R}^{\dagger})_{lj}; \tag{27}$$

$$\xi_{ij}^{D(\ell)} = (V_{D(\ell),L})_{ik} (-s_{\beta} e^{-i\xi} (Y_{1d(\ell)})_{kl} + c_{\beta} (Y_{2d(\ell)})_{kl}) (V_{D(\ell),R}^{\dagger})_{lj}. \tag{28}$$

The off-diagonal elements of $\xi_{ij}^{U,D,\ell}$ induce the flavor changing processes at tree level. It was proved in [1] that in the $t_{\beta} s_{\xi} \rightarrow 0$ limit, all the four quantities $m_{\eta}, c_{\eta,V}, K, J \propto t_{\beta} s_{\xi}$ which means the correlation between the lightest scalar and smallness of CP-violation.

In the scenario we discuss in this paper, there can be exotic Higgs decay channels $h \rightarrow \eta\eta, Z\eta$ induced by

$$\mathcal{L}_{\text{exo}} = \frac{c_{h\eta} g}{2c_W} (h \partial_{\mu} \eta - \eta \partial_{\mu} h) Z^{\mu} - \frac{1}{2} g_{h\eta\eta} v h \eta^2. \tag{29}$$

It leads to the branching ratios

$$\text{Br}(h \rightarrow Z\eta) = \frac{g^2 c_{h\eta}^2 m_h^3}{64\pi m_W^2 \Gamma_{h,\text{tot}}} \mathcal{F}\left(\frac{m_Z^2}{m_h^2}, \frac{m_{\eta}^2}{m_h^2}\right); \tag{30}$$

$$\text{Br}(h \rightarrow \eta\eta) = \frac{g_{h\eta\eta}^2 v^2}{32\pi m_h \Gamma_{h,\text{tot}}} \sqrt{1 - \frac{4m_{\eta}^2}{m_h^2}} \tag{31}$$

where $\mathcal{F}(x, y) = (1 + x^2 + y^2 - 2x - 2y - 2xy)^{3/2}$, g is the weak coupling constant and $c_W \equiv m_W/m_Z$. For the detail couplings, please see section A in appendices, in which all $c_{h,f}$ are defined as the ratio between Higgs- $f\bar{f}$ couplings and those in SM.

III. CONSTRAINTS FOR THIS SCENARIO BY RECENT DATA

Besides the 125 GeV Higgs boson (h), there are two extra neutral scalars and one of which is expected to be light in this scenario. For the lightest scalar η with its mass $m_{\eta} \sim \mathcal{O}(0.1 - 1)\text{GeV}$, the BESIII [42], BaBar [43, 44] and CMS [45] experiments gave strict

constraints thus we will focus on the cases $m_\eta \sim \mathcal{O}(10)\text{GeV}$. Type II 2HDM including a light scalar with mass $(25 - 80)\text{GeV}$ is excluded [46] through the search for $\eta b\bar{b}$ associated production. While for a general case it is still allowed by collider data, as we will show below. The two extra scalars would face the constraints from the direct searches at LEP and LHC. In this scenario of Lee model, with a light particle η , the exotic decay channels $h \rightarrow \eta\eta, Z\eta$ will modify the total width and signal strengths for the 125 GeV Higgs boson that we should also consider the constraints from Higgs signal strengths.

In Lee model, there is no additional discrete symmetry to forbid flavor changing processes at tree level, and there are also new origins for CP-violation. Thus it must face the constraints in flavor physics, including rare decays, meson mixing, etc. The electric dipole moments (EDM) for electron [47] and neutron [48] would also give strict constraints in many models with additional CP-violation source [49] including Lee model, so we must consider the EDM constraints here as well.

A. Direct Searches for Extra Scalars

The LEP experiments [50–52] set strict constraints on this scenario through the $e^+e^- \rightarrow Z\eta$ and $e^+e^- \rightarrow h\eta$ associated production processes. For η with its mass $(15 - 40)\text{GeV}$, [50, 51] gave $\sigma_{Z\eta}/\sigma_{\text{SM}} \lesssim (1.5 - 4) \times 10^{-2}$ at 95% C.L. which meant

$$c_{\eta,V} \lesssim (0.12 - 0.2) \quad (32)$$

thus $t_\beta s_\xi \lesssim 0.1$ in this scenario. At the same mass region for η , assuming both η and h decay to $b\bar{b}$ final states dominantly, [51, 52] gave $c_{h\eta}^2 \lesssim (0.2 - 0.3)$. According to (A.15), $c_{H,V} = c_{h\eta}$ thus $c_{H,V}$ should also be small. The results implied that $c_{h,V} \sim 1$ thus the couplings of h should be SM-like.

The direct searches for a heavy Higgs boson at LHC [53, 54] excluded a SM Higgs boson in the mass region $(145 - 1000)\text{GeV}$ at 95% C.L. A SM Higgs boson with its mass around v would decay to WW and ZZ final states dominantly with $\text{Br}(H_{\text{SM}} \rightarrow VV) \approx 1$ [55], while in 2HDM it can be modified because of a suppressed HVV coupling and the existence of other decay channels like $H \rightarrow Z\eta, \eta\eta, h\eta$, and Zh (if $m_H > m_Z + m_h = 216\text{GeV}$), hh (if $m_H > 2m_h = 250\text{GeV}$), H^+H^- (if $m_H > 2m_\pm$). For a heavy scalar H , analytically the

partial widths should be

$$\Gamma_H(VV) \approx c_{H,V}^2 \Gamma_{H,SM}; \quad (33)$$

$$\Gamma_H(\eta\eta) = \frac{g_{H\eta\eta}^2 v^2}{32\pi m_H} \sqrt{1 - \frac{4m_\eta^2}{m_H^2}}; \quad (34)$$

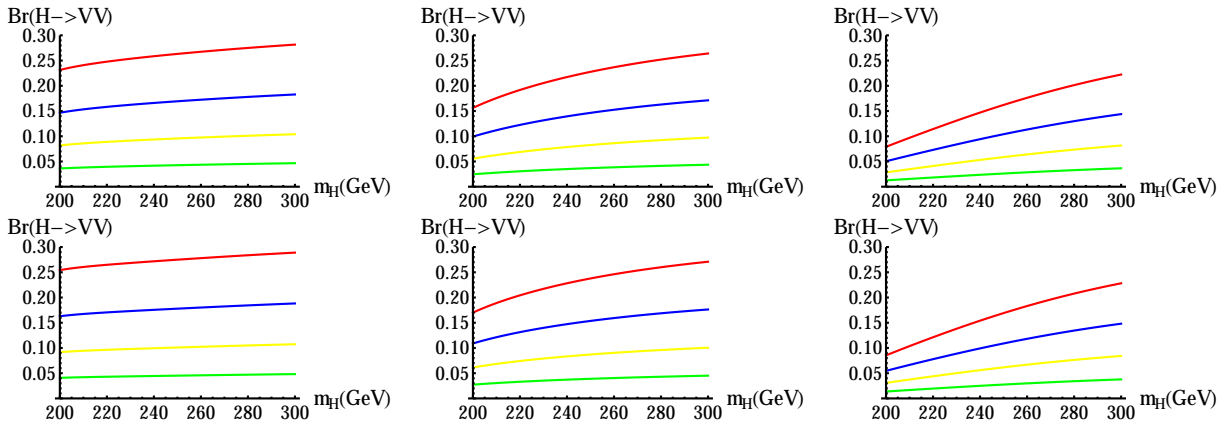
$$\Gamma_H(Z\eta) = \frac{c_{h,V}^2 m_H^3}{8\pi v^2} \mathcal{F}\left(\frac{m_\eta^2}{m_H^2}, \frac{m_Z^2}{m_H^2}\right). \quad (35)$$

The suppression in $\Gamma_H(VV)$ comes from small $c_{H,V}$ while $\Gamma_H(Z\eta) \propto c_{h,V}^2$ is not suppressed because h is SM-like and $c_{h,V} \sim 1$. According to CMS results [53] which gave the most strict constraint, for $m_H \sim (200 - 300)\text{GeV}$, the 95% C.L. upper limit for the signal strength is ⁷

$$\mu_H \equiv \frac{\sigma_H}{\sigma_{H,SM}} \cdot \frac{\text{Br}(H \rightarrow VV)}{\text{Br}_{SM}(H \rightarrow VV)} \lesssim (0.1 - 0.2). \quad (36)$$

Numerically, we show the $\text{Br}(H \rightarrow VV) - m_H$ plots for different parameter choices fixing $c_{\eta,V} = 0.1$ in Figure 1. From the figures, we can see that if the production cross section

FIG. 1: $\text{Br}(H \rightarrow VV) - m_H$ plots for different parameter choices fixing $c_{\eta,V} = 0.1$. The green, yellow, blue, and red lines stand for $c_{H,V} = 0.2, 0.3, 0.4, 0.5$ respectively in each figure. The upper figures are for $m_\eta = 20\text{GeV}$ while the lower figures are for $m_\eta = 40\text{GeV}$. In each line, from left to right, we take $g_{H\eta\eta} = 0, 0.5, 1$.



$\sigma_H \sim \sigma_{H,SM}$, $c_{H,V} \lesssim 0.3$ would be allowed; while if $\sigma_H \sim 0.5\sigma_{H,SM}$, $c_{H,V} \lesssim 0.4$ would also be allowed. It is not sensitive to m_η . We did not consider the $H \rightarrow hh$ channel for $m_H > 2m_h = 250\text{GeV}$ in the discussions above. Numerically, for $g_{Hhh} \sim 1$, we have $\text{Br}(H \rightarrow hh) \lesssim 0.1$ which leads to $\sigma(pp \rightarrow H \rightarrow hh) \lesssim 0.4\text{pb}$ [55]. For this case, the direct

⁷ For a heavy Higgs boson, $\text{Br}_{SM}(H \rightarrow VV) \sim 1$ according to [55].

search for $H \rightarrow hh$ channel by CMS [56] cannot give further constraint. We don't consider the case $m_H \gg v$ here because of the weakly-coupled hypothesis.

No significant evidence for a charged Higgs boson had been found at colliders. Recently the ATLAS searches through $gb \rightarrow tH^- (\rightarrow t\bar{b})$ process gave constraint on the tbH^\pm vertex as [57]

$$|\xi_{tt}| \lesssim (1.5 - 3) \quad (37)$$

for a charged Higgs boson with mass m_\pm in the region $(200 - 600)\text{GeV}$. In these searches, some hints for a charged Higgs signal with about 2.4σ significance were also found in this mass region. As can be seen below, it is consistent with this scenario.

B. Global-fits for Higgs Signal Strengths

The Higgs signal strength for a channel which exists in SM is defined as

$$\mu_{i,f} \equiv \frac{\sigma \cdot \text{Br}}{(\sigma \cdot \text{Br})_{\text{SM}}} = \frac{\sigma_i}{\sigma_{i,\text{SM}}} \cdot \frac{\Gamma_h(f)}{\Gamma_{h,\text{SM}}(f)} \cdot \frac{\Gamma_{h,\text{tot,SM}}}{\Gamma_{h,\text{tot}}}. \quad (38)$$

The SM Higgs boson with its mass $m_h = 125\text{GeV}$ has a total width $\Gamma_{h,\text{tot,SM}} = 4.1\text{MeV}$ [55]. In this scenario, $\Gamma_{h,\text{tot}}$ is also modified by the exotic decay channels $h \rightarrow Z\eta, \eta\eta$. Here for VBF or Vh associated production channel, $\sigma/\sigma_{\text{SM}} = c_{h,V}^2$; while for gluon fusion production,

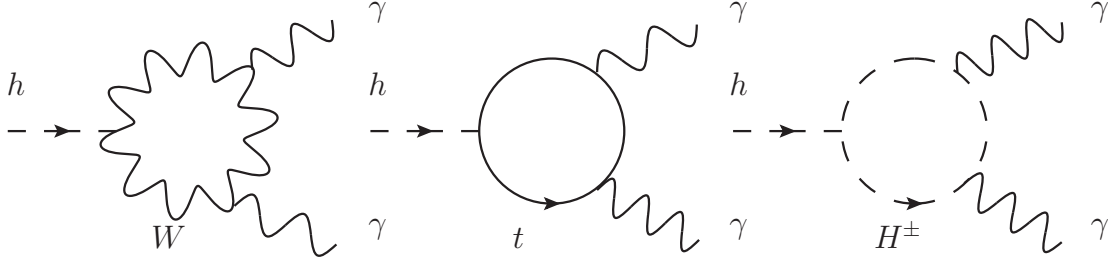
$$\frac{\sigma}{\sigma_{\text{SM}}} = \left| \text{Re}(c_{h,t}) + i \frac{\mathcal{B}_{1/2}(x_t)}{\mathcal{A}_{1/2}(x_t)} \text{Im}(c_{h,t}) \right|^2. \quad (39)$$

For the decay channels $h \rightarrow WW^*$ and ZZ^* , we have $\Gamma_h(VV)/\Gamma_{h,\text{SM}}(VV) = c_{h,V}^2$; for $h \rightarrow b\bar{b}, c\bar{c}$ and $\tau^+\tau^-$, $\Gamma_h(f)/\Gamma_{h,\text{SM}}(f) = |c_{h,f}|^2$; while for the loop induced decay processes,

$$\frac{\Gamma_h(gg)}{\Gamma_{h,\text{SM}}(gg)} = \left| \text{Re}(c_{h,t}) + i \frac{\mathcal{B}_{1/2}(x_t)}{\mathcal{A}_{1/2}(x_t)} \text{Im}(c_{h,t}) \right|^2; \quad (40)$$

$$\frac{\Gamma_h(\gamma\gamma)}{\Gamma_{h,\text{SM}}(\gamma\gamma)} = \left| \frac{c_{h,V}\mathcal{A}_1(x_W) + \frac{4}{3}\text{Re}(c_{h,t})\mathcal{A}_{1/2}(x_t) + \left(\frac{g_{h,\pm}v^2}{2m_\pm^2}\right)\mathcal{A}_0(x_\pm) + \frac{4}{3}i\text{Im}(c_{h,t})\mathcal{B}_{1/2}(x_t)}{\mathcal{A}_1(x_W) + \frac{4}{3}\mathcal{A}_{1/2}(x_t)} \right|^2. \quad (41)$$

Here $x_i \equiv m_h^2/4m_i^2$ where i denotes the particles t, W or H^\pm in loops. The index j in $\mathcal{A}(\mathcal{B})_j$ denotes the spin of the particle in loops, see the Feynman diagrams in Figure 2. The

FIG. 2: Feynman diagrams for $h \rightarrow \gamma\gamma$ decay in this model.

analytical loop integration functions given by [58, 59] are listed in section B as (B.1)-(B.5). According to [55],

$$\begin{aligned} \Gamma_{h,\text{tot}} = & \Gamma_{h,\text{tot,SM}} \left(0.58|c_{h,b}|^2 + 0.24c_{h,V}^2 + 0.06|c_{h,\tau}|^2 + 0.03|c_{h,c}|^2 \right. \\ & \left. + 0.09|c_{h,t}|^2(1 + 1.31 \sin^2 \alpha_t) \right) + \Gamma_{h,\text{exo}} \end{aligned} \quad (42)$$

where $\Gamma_{h,\text{tot,SM}} = 4.1\text{MeV}$ for $m_h = 125\text{GeV}$. $\alpha_t \equiv \arg(c_{h,t})$ and $\Gamma_{h,\text{exo}}$ is the exotic decay width. Define

$$\chi^2 \equiv \sum_{i,f} \left(\frac{\mu_{i,f,\text{obs}} - \mu_{i,f,\text{pre}}}{\sigma_{i,f}} \right)^2 \quad (43)$$

ignoring the correlations between different channels. $\mu_{i,f,\text{obs(pre)}}$ means the observed (predicted) signal strength for production channel i and decay final state f and $\sigma_{i,f}$ means the standard deviation of the signal strength measurement for the corresponding channel. Numerically, the fitting results are not sensitive to the charged Higgs contribution in $h \rightarrow \gamma\gamma$ channel.

According to (A.21), in this scenario, $c_{h,f} \sim 1$ holds for all fermions since h contains large component of R_1 . Thus for all $c_{h,f}$, the modifications from 1 are suppressed by t_β . We also have $c_{h,V} \sim 1$ in the text above. Thus for any channel, according to (38)

$$\mu_{i,f,\text{pre}} = \frac{\sigma_i}{\sigma_{i,\text{SM}}} \cdot \frac{\Gamma_h(f)}{\Gamma_{h,\text{SM}}(f)} \cdot \frac{\Gamma_{h,\text{tot,SM}}}{\Gamma_{h,\text{tot}}} \sim \frac{\Gamma_{h,\text{tot,SM}}}{\Gamma_{h,\text{tot}}}, \quad (44)$$

which means the signal strengths are mainly modified by the exotic decay width Γ_{exo} . Numerically $\Gamma_{\text{exo}} \lesssim (1-2)\text{MeV}$ is still allowed for other couplings close to those in SM. For $m_\eta < m_h/2$, $h \rightarrow \eta\eta$ channel is available. And according to (31), we have

$$g_{h\eta\eta} \lesssim \mathcal{O}(10^{-2}) \quad (45)$$

which means a strong correlation among λ_i in Higgs potential. To the leading order ,

$$g_{h\eta\eta} = (\lambda_3 + \lambda_7)c_\theta + \frac{1}{2}\lambda_5 s_\theta + \mathcal{O}(t_\beta s_\xi), \quad (46)$$

which gives $\lambda_3 + \lambda_7 \simeq -\lambda_5 t_\theta/2 + \mathcal{O}(t_\beta s_\xi)$. While for $m_\eta < m_h - m_Z$, $h \rightarrow Z\eta$ channel is open, (30) gave

$$c_{H,V} = c_{h\eta} \lesssim \mathcal{O}(10^{-2} - 10^{-1}). \quad (47)$$

For $m_\eta \sim (15 - 30)\text{GeV}$, $c_{h\eta} = 0.05$ is still allowed.

According to the direct searches for heavy neutral Higgs boson H , we can see that $c_{H,V} = 0.3$ is in the allowed region for almost all cases. While according to the bounds from Higgs signal strengths, we can see for $m_\eta < m_h - m_Z = 34\text{GeV}$, there would be further constraint on $c_{H,V}$ from $h \rightarrow Z\eta$ rare decay channel. In this case, $c_{H,V} = 0.05$ would be allowed. Thus we have two groups of typical benchmark points as listed in Table I. We choose $m_\eta = 20\text{GeV}$ and 40GeV as the two typical cases.

TABLE I: Benchmark points in scalar sector for the following parts of this paper. The first line is a typical choice for the case $h \rightarrow Z\eta$ decay allowed; while the second line is a typical choice for the case $h \rightarrow Z\eta$ decay forbidden.

Case	m_η	m_H	$c_{h,f}$	$c_{\eta,V}$	$c_{H,V}$	$c_{h,V}$	$t_\beta s_\xi$
I	20 GeV	$\sim v$	~ 1	0.1	0.05	0.994	~ 0.1
II	40 GeV	$\sim v$	~ 1	0.1	0.3	0.95	~ 0.1

C. Constraints from Oblique Parameters

The GFitter group gave updated electro-weak fitting results [60] for oblique parameters [61] as

$$S = 0.05 \pm 0.11, \quad T = 0.09 \pm 0.13, \quad U = 0.01 \pm 0.11, \quad (48)$$

$$R_{ST} = +0.90, \quad R_{SU} = -0.59, \quad R_{TU} = -0.83;$$

where R means the correlation between two variables. Here U is also treated as a free variable and the reference points are taken as $m_{h,\text{ref}} = 125\text{GeV}$, $m_{t,\text{ref}} = 173\text{GeV}$. In 2HDM, U is expected to be ignorable thus we can fix $U = 0$ and get [60]

$$S = 0.06 \pm 0.09, \quad T = 0.10 \pm 0.07, \quad R = +0.91. \quad (49)$$

In 2HDM, the contribution to δS and δT [3, 62, 63] are

$$\delta S = \frac{1}{24\pi} \left[(1 - 2s_W^2)^2 G(z_\pm, z_\pm) + c_1^2 G(z_2, z_3) + c_2^2 G(z_3, z_1) + c_3^2 G(z_1, z_2) \right. \\ \left. + \sum_{i=1}^3 \left(c_i^2 H(z_i) + \ln \left(\frac{m_i^2}{m_{H^\pm}^2} \right) \right) - H \left(\frac{m_{h,\text{ref}}^2}{m_Z^2} \right) - \ln \left(\frac{m_{h,\text{ref}}^2}{m_{H^\pm}^2} \right) \right]; \quad (50)$$

$$\delta T = \frac{1}{16\pi s_W^2 m_W^2} \left[\sum_{i=1}^3 (1 - c_i^2) F(m_{H^\pm}^2, m_i^2) - c_1^2 F(m_2^2, m_3^2) - c_2^2 F(m_3^2, m_1^2) - c_3^2 F(m_1^2, m_2^2) \right. \\ \left. + 3 \sum_{i=1}^3 c_i^2 (F(m_Z^2, m_i^2) - F(m_W^2, m_i^2)) - 3(F(m_Z^2, m_{h,\text{ref}}^2) - F(m_W^2, m_{h,\text{ref}}^2)) \right]. \quad (51)$$

The arguments above are defined as $z_i \equiv (m_i/m_Z)^2$ and $z_\pm \equiv (m_\pm/m_Z)^2$. The analytical loop integration functions given by [3, 62, 63] are listed in section B as (B.6)-(B.9).

We perform the fitting process based on the mathematica code [64]⁸ with the benchmark points in Table I. We plot the curves using the charged Higgs mass m_\pm as a parameter in Figure 3. Direct searches by LEP gave constraints on charged Higgs boson mass as $m_\pm > 78.6\text{GeV}$ [65] at 95% C.L. so that we begin from $m_\pm = 80\text{GeV}$. The thick regions in the curves stands for allowed regions by oblique parameter constrains for both benchmark points. For both cases in Table I, we list the allowed m_\pm in Table II. For all the cases,

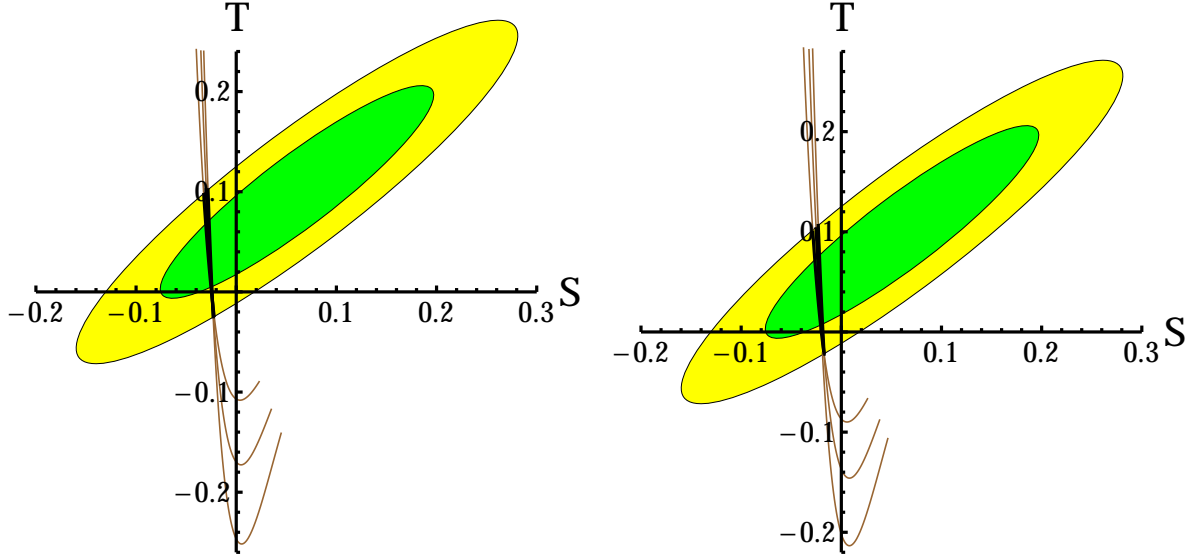
TABLE II: Allowed regions for m_\pm for each case above.

m_H (GeV)	200	250	300
Allowed m_\pm for Case I (GeV)	190 – 231	242 – 277	293 – 323
Allowed m_\pm for Case II (GeV)	185 – 228	232 – 269	279 – 311

allowed m_\pm are around the heavy neutral Higgs mass m_H , as the scenario discussed by [16, 66]. For m_H around the electro-weak scale v , a charged Higgs boson should also have its mass around that scale. A light charged Higgs boson (with its mass $m_\pm < m_t$) is disfavored here thus we don't consider the constraints from the rare decay process $t \rightarrow H^+ b$.

⁸ The second χ^2 (for 95% C.L.) should be 6.0 according to [29].

FIG. 3: Oblique parameter constraints for the scenario we discussed in this paper. The green region is 68% C.L. allowed and the yellow region is 95% C.L. allowed. The left figure is for Case I while the right figure is for Case II in Table I. We plot the curves with a parameter m_{\pm} . In each curve, we begin with $m_{\pm} = 80\text{GeV}$. In both figures, the curves from left to right are for $m_H = (200, 250, 300)\text{GeV}$ respectively. For the allowed regions in the curves, we made them thick and black, please see the allowed regions in Table II in details.



D. Constraints from Meson Mixing Data

The neutral mesons K^0 , D^0 , B^0 , and B_s^0 should mix with their anti-particles through W^{\pm} mediated box diagrams in the SM. Thus a nontrivial contribution to $\langle \bar{M}^0 | \mathcal{H} | M^0 \rangle$ leads to the mass splitting effect between different CP eigenstates for meson⁹. Here we list the experimental data [29, 67] and SM predictions [68–71]¹⁰ for meson mixing in Table III where the decay constants and bag parameters are from lattice data [72].

TABLE III: Experimental data and SM predictions for mass splitting effects in meson mixing.

⁹ In fact in the real world, CP is not a good symmetry thus a mass eigenstate is modified a little from a CP eigenstate. See the details for this formalism in section C.

¹⁰ No SM prediction results for Δm_D appears because the dominant contribution comes from long-distance interactions thus it is difficult to calculate.

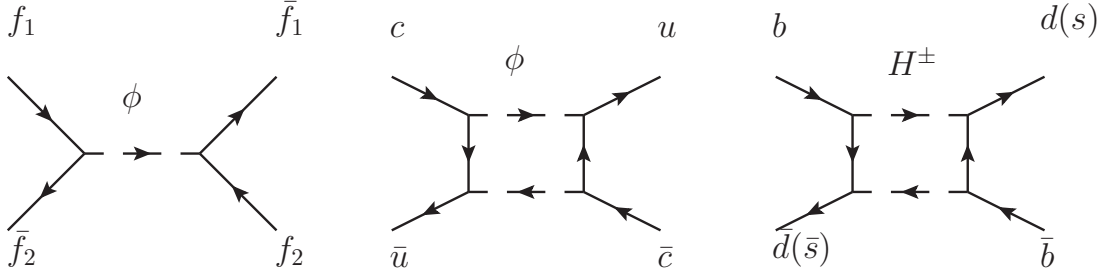
Meson	Δm_{exp} (GeV)	Δm_{SM} (GeV)
$K^0(d\bar{s})$	$(3.483 \pm 0.006) \times 10^{-15}$	$(3.30 \pm 0.34) \times 10^{-15}$
$D^0(c\bar{u})$	$(5.9 \pm 2.6) \times 10^{-15}$	—
$B_d^0(d\bar{b})$	$(3.36 \pm 0.02) \times 10^{-13}$	$(3.57 \pm 0.60) \times 10^{-13}$
$B_s^0(s\bar{b})$	$(1.1686 \pm 0.0014) \times 10^{-11}$	$(1.14 \pm 0.17) \times 10^{-11}$

In general, we can parameterize the off-diagonal element in mass matrix as [73, 74]

$$\mathbf{m}_{12,M} \equiv \frac{1}{2m_M} \langle \bar{M}^0 | \mathcal{H} | M^0 \rangle = \mathbf{m}_{12,M}^{\text{SM}} (1 + \Delta_M e^{2i\delta_M}) \quad (52)$$

where the factor $(2m_M)^{-1}$ comes from the normalization condition. In SM we must have $\Delta_M = \delta_M = 0$. In $B^0(B_s^0)$ system, $\Delta m_{B(B_s)} = 2|\mathbf{m}_{12,B(B_s)}|$; while in K^0 system, $\Delta m_K = 2\text{Re}(\mathbf{m}_{12,K})$. A nonzero δ_M would also modify the CP-violation effects from those in SM. In Lee model, the additional contributions to $\mathbf{m}_{12,M}$ are shown in Figure 4. The neutral

FIG. 4: Additional Feynman diagrams contributed to $\mathbf{m}_{12,M}$ in Lee model.



scalars $\phi = \eta, h, H$ in the diagrams.

First, consider the left diagram in Figure 4 which induce the mixing directly at tree level. It can contribute to the mixing of all the four kinds of mesons. The dominant contribution must come from η because it is light and its flavor changing couplings are not suppressed by $t_\beta s_\xi$ or s_θ . The tree level η induced contribution for $M^0(f_i \bar{f}_j) - \bar{M}^0(f_j \bar{f}_i)$ mixing is [75, 76]

$$\mathbf{m}_{12,M}^{\eta, \text{tree}} = \frac{f_M^2 B_M m_M m_i m_j}{12m_\eta^2 v^2} \left[\left(1 + \frac{6m_M^2}{(m_i + m_j)^2} \right) c_{\eta,ij} c_{\eta,ji}^* - \frac{5m_M^2}{2(m_i + m_j)^2} (c_{\eta,ij}^2 + c_{\eta,ji}^{*2}) \right]. \quad (53)$$

Here f_M and B_M are the decay constant and bag parameter for meson M^0 separately. According to (A.23), $c_{\eta,ij} = \pm \xi_{ij} (1 + \mathcal{O}(t_\beta s_\xi))$. With the experimental constraints in [74, 77], for different $\delta_{B(B_s)}$, $\Delta_{B(B_s)} \lesssim (0.1 - 0.4)$ at 95% C.L. Assuming $|\xi_{ij}| \sim |\xi_{ji}|$, numerically

for $m_\eta \sim (20 - 40)\text{GeV}$, we have

$$|\xi_{bd(db)}| \lesssim (0.7 - 3) \times 10^{-2}, \quad |\xi_{bs(sb)}| \lesssim (0.9 - 2.5) \times 10^{-2}. \quad (54)$$

Similarly, $|\xi_{sd(ds)}| \lesssim (0.8 - 1.7) \times 10^{-2}$ for $K^0 - \bar{K}^0$ mixing from [74]. While for $D^0 - \bar{D}^0$ mixing, we have $|\xi_{cu(uc)}| \lesssim (1.7 - 3.4) \times 10^{-2}$. For all the four types of mixing, the constraints on ξ_{ij} are of $\mathcal{O}(10^{-2})$.

Next, consider the middle diagram in Figure 4 which can induce a $D^0 - \bar{D}^0$ mixing through top quark and a scalar mediated in the box. Assuming $|\xi_{tu(c)}| \sim |\xi_{u(c)t}|$, its contribution to Δm_D is [78]

$$\Delta m_D^{\eta, \text{box}} \approx \frac{m_u m_c |\xi_{tu} \xi_{tc}|^2}{24\pi^2 v^4} f_D^2 m_D B_D r \mathcal{F}_0 \left(\frac{m_t^2}{m_\eta^2} \right) \quad (55)$$

where $r = (\alpha_s(m_t)/\alpha_s(m_b))^{6/23}(\alpha_s(m_b)/\alpha_s(m_c))^{6/25} = 0.8$ describes the QCD effects and loop function $\mathcal{F}_0(x)$ [78] is listed as (B.10) in section B in the appendices. Assuming its contribution is less than the complete Δm_D , numerically we have

$$|\xi_{tu} \xi_{tc}| \lesssim 6 \quad (56)$$

for a η with its mass $(20 - 40)\text{GeV}$.

Last, consider the right diagram in Figure 4 which induce $B^0(B_s^0) - \bar{B}^0(\bar{B}_s^0)$ mixing through the box diagram in which one or two W^\pm should be replaced by H^\pm comparing with the case in SM. This kind of diagrams are highly suppressed in $K^0 - \bar{K}^0$ mixing. In neutral B sector, the contributions from $W^\pm - H^\pm$ box and H^\pm box can be estimated as [79]

$$\Delta_{B(B_s)} e^{i\delta_{B(B_s)}} = \xi_{tt}^2 \cdot \frac{\mathcal{F}_1(m_t^2/m_W^2, m_t^2/m_\pm^2, m_\pm^2/m_W^2) + \xi_{tt}^2 \mathcal{F}_0(m_t^2/m_\pm^2)}{\mathcal{F}_2(m_t^2/m_W^2)}. \quad (57)$$

The loop functions \mathcal{F}_i [79] are listed as (B.10)-(B.12) in section B in the appendices, and \mathcal{F}_0 is the same as that in the box diagram for $D^0 - \bar{D}^0$ mixing in (55). It is sensitive only to ξ_{tt} because the other terms are suppressed by the mass of down type quarks. The S-T parameter fits favor a charged Higgs boson with mass $m_\pm \sim m_H \sim v$ (see also Table II), so numerically we have

$$|\xi_{tt}| \lesssim (0.6 - 0.9) \quad (58)$$

using the $B^0(B_s^0) - \bar{B}^0(\bar{B}_s^0)$ mixing constraints [74, 77]. This bound is stricter than that from the direct searches for a charged Higgs boson in (37).

E. LHC Constraints on Top Quark Flavor Violation

The ϕtq (where $q = c, u$ and $\phi = \eta, h$) direct interactions in (A.23) and (A.24) would induce $t \rightarrow \phi q$ rare decay processes. The partial widths can be given by

$$\Gamma(t \rightarrow \phi q) = \frac{m_t^2 m_q (|c_{\phi, tq}|^2 + |c_{\phi, qt}|^2)}{32\pi v^2} \left(1 - \frac{m_\phi^2}{m_t^2}\right)^2. \quad (59)$$

For $\phi = \eta$, we have $c_{\eta, ij} = i\xi_{ij} + \mathcal{O}(t_\beta s_\xi) \sim i\xi_{ij}$; while for $\phi = h$, if $m_\eta < 34\text{GeV}$, $c_{h, ij} \sim -it_\beta s_\xi \xi_{ij} \sim -0.1i\xi_{ij}$ with $t_\beta s_\xi \sim 0.1$; else $c_{h, ij} \sim (-0.1i + \mathcal{O}(0.1))\xi_{ij}$. For the latter case,

$$|c_{h, ij}| \sim (0.1 - 0.3)|\xi_{ij}|. \quad (60)$$

All the numerical estimations above are based on (A.23) and (A.24) etc. in section A. The combined experimental result by ATLAS [80] gave

$$\text{Br}(t \rightarrow hc) < 0.46\% \quad \text{and} \quad \text{Br}(t \rightarrow hu) < 0.45\% \quad (61)$$

respectively at 95% C.L. Assuming $|\xi_{ij}| \sim |\xi_{ji}|$ as usual, we have

$$|\xi_{tu}| \lesssim (1 - 3) \times 10^2 \quad \text{and} \quad |\xi_{tc}| \lesssim (5 - 14) \quad (62)$$

using the SM predicted top quark total width $\Gamma_{t, \text{tot}} \approx 1.3\text{GeV}$ [29, 81].

It is difficult to search for $t \rightarrow \eta q$ rare decay since η decays to jets dominantly, but we can obtain the constraints through the exotic decay branching ratio of top quark. The $t\bar{t}$ production cross section measurements at LHC with $\sqrt{s} = 8\text{TeV}$ gave $\sigma_{t\bar{t}} = (237 \pm 13)\text{pb}$ [82] assuming $m_t = 173\text{GeV}$ and $\text{Br}(t \rightarrow Wb) = 1$, which is consistent with the SM prediction $\sigma_{t\bar{t}, \text{SM}} = (246_{-11}^{+9})\text{pb}$ [83]. Thus we have for the top exotic decay channels that $\Gamma(t \rightarrow \text{exotic})/\Gamma(t \rightarrow Wb) < 8\%$ at 95% C.L. In this scenario, $\text{Br}(t \rightarrow \eta q)/\text{Br}(t \rightarrow hq) \sim \mathcal{O}(10 - 10^2)$, thus $t \rightarrow hq$ is ignorable in this paragraph. With these data, we have

$$2 \times 10^{-4} |\xi_{tu}|^2 + 0.1 |\xi_{tc}|^2 \lesssim 1 \quad (63)$$

for $m_\eta \sim (20 - 40)\text{GeV}$.

The last constraint comes from same sign top production. The 95% C.L. upper limit given by CMS [84] is $\sigma_{tt} < 0.37\text{pb}$. Theoretically, η mediated $uu \rightarrow tt$ process would be the dominant production channel in this scenario. The cross section can be expressed as

$$\sigma(uu \rightarrow tt) = \int dx_1 dx_2 f_u(x_1) f_u(x_2) \sigma(s_0) \quad (64)$$

where $f_u(x)$ is the parton distribution function (PDF) for up quark and

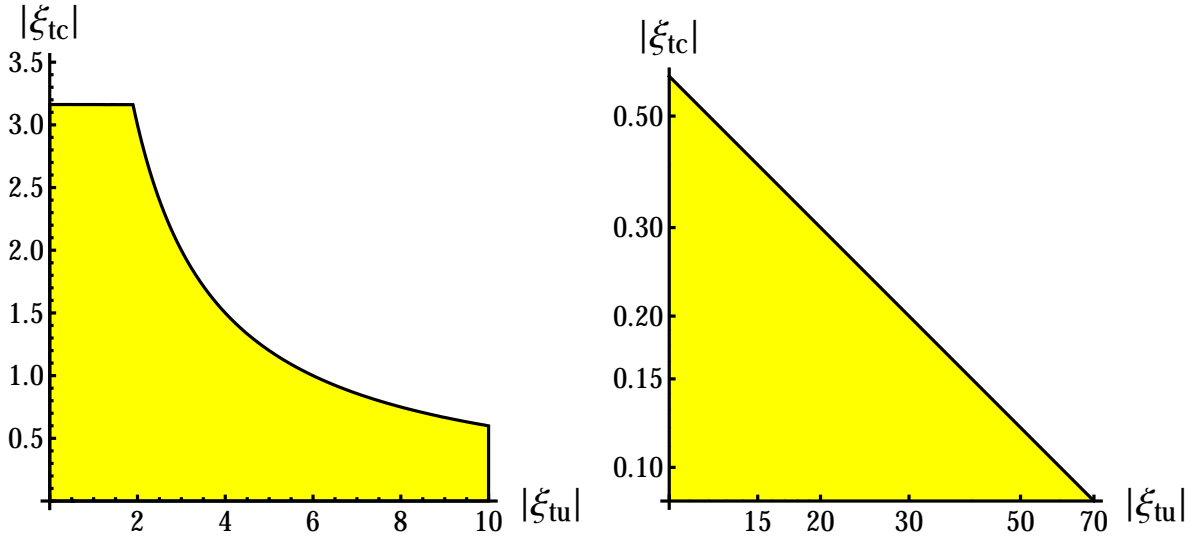
$$\sigma(s_0) = \frac{m_u^2 m_t^2 \beta_t (|\xi_{tu}|^2 + |\xi_{ut}|^2)^2}{64\pi s_0 v^4} \int_{-1}^1 dc_\theta \left[\left(\frac{1 - \beta_t c_\theta}{1 + \beta_t^2 + 4m_\eta^2/s_0 - 2\beta_t c_\theta} \right)^2 \right. \\ \left. \left(\frac{1 + \beta_t c_\theta}{1 + \beta_t^2 + 4m_\eta^2/s_0 + 2\beta_t c_\theta} \right)^2 - \frac{1 + \beta_t^2 (c_\theta^2 - 2)}{(1 + \beta_t^2 + 4m_\eta^2/s_0)^2 - 4\beta_t^2 c_\theta^2} \right]. \quad (65)$$

Here $s_0 \equiv x_1 x_2 s_{\text{LHC}}$ is the square of energy in the moment center frame of two partons; $\beta_t \equiv \sqrt{1 - 4m_t^2/s_0}$ is the velocity of top quark and θ is the azimuth angle of top quark in respect to the beam line. Numerically, for $m_\eta \sim (20 - 40)\text{GeV}$, assuming $|\xi_{tu}| \sim |\xi_{ut}|$ and using the MSTW2008 PDF [85], we have

$$|\xi_{tu}| \lesssim 10^2. \quad (66)$$

Combining the equations (56), (62), (63), and (66), we plot the estimations of allowed region in the $|\xi_{tu}| - |\xi_{tc}|$ plane in Figure 5. The strictest upper limit $|\xi_{tc}| \lesssim 3$ and $|\xi_{tu}| \lesssim 70$ comes from (63), and the obvious behavior of the correlation between $|\xi_{tc}|$ and $|\xi_{tu}|$ comes from (56). The boundary contains relative errors of $\mathcal{O}(10\%)$ and it is not sensitive to m_η for $m_\eta \sim (20 - 40)\text{GeV}$.

FIG. 5: Allowed region for top flavor changing couplings. Notice in the right figure we used double-log coordinates to show a very large region.



F. Constraints on Lepton Flavor Violation

In type III 2HDM [37] there exist direct $\ell_i \ell_j \phi$ vertices to be constrained. For the discovered 125 GeV Higgs boson, a straightforward calculation gives [86]

$$\text{Br}(h \rightarrow \ell_i^\pm \ell_j^\mp) = \frac{m_h m_i m_j}{8\pi \Gamma_h v^2} (|c_{h,ij}|^2 + |c_{h,ji}|^2). \quad (67)$$

For $h \rightarrow \mu\tau$ process, direct searches by CMS [86] and ATLAS [87] collaborations gave $\text{Br}(h \rightarrow \mu\tau) < 1.51\%$ and $\text{Br}(h \rightarrow \mu\tau) < 1.85\%$ respectively, both at 95% C.L.¹¹ In this scenario, $|c_{h,ij}|$ is suppressed to be $(0.1 - 0.3)|\xi_{ij}|$ for $m_\eta \sim (20 - 40)\text{GeV}$, assuming $|c_{h,ij}| \sim |c_{h,ji}|$, we have the bound

$$|\xi_{\mu\tau}| \lesssim (5 - 16). \quad (68)$$

Another kind of strict constraints on $\ell_i \ell_j \phi$ vertices come from radiative LFV decays as $\tau \rightarrow \mu\gamma$ and $\mu \rightarrow e\gamma$. For $\tau \rightarrow \mu(e)\gamma$, Belle and BaBar collaborations gave the 90% C.L. upper limit as [88, 89]

$$\text{Br}(\tau \rightarrow \mu\gamma) < 4.5 \times 10^{-8}, \quad \text{Br}(\tau \rightarrow e\gamma) < 1.2 \times 10^{-7} \quad (\text{Belle}); \quad (69)$$

$$\text{Br}(\tau \rightarrow \mu\gamma) < 4.4 \times 10^{-8}, \quad \text{Br}(\tau \rightarrow e\gamma) < 3.3 \times 10^{-8} \quad (\text{BaBar}). \quad (70)$$

While for $\mu \rightarrow e\gamma$, the MEG collaboration gave [90]

$$\text{Br}(\mu \rightarrow e\gamma) < 5.7 \times 10^{-13} \quad (71)$$

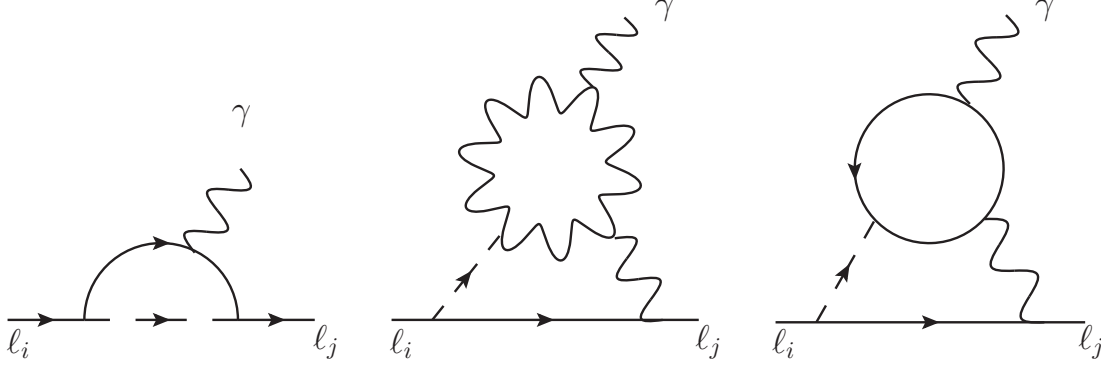
at 90% C.L. In SM, the branching ratios of $\ell_i \rightarrow \ell_j \gamma$ processes are estimated to be of $\mathcal{O}(10^{-56} - 10^{-54})$ [29, 91, 92] which are far below the experimental sensitivity. But in 2HDM with LFV, it can be larger or even comparable to recent data. In this model, $\ell_i \rightarrow \ell_j \gamma$ process can be generated by Feynman diagrams in Figure 6 and the branching ratios can be expressed as [93]

$$\frac{\text{Br}(\ell_i \rightarrow \ell_j \gamma)}{\text{Br}(\ell_i \rightarrow \ell_j \nu_i \bar{\nu}_j)} = \frac{48\pi^3 \alpha}{G_F^2} (|A_L|^2 + |A_R|^2) \quad (72)$$

where $A_{L(R)}$ are defined through [94, 95]

$$\mathcal{M}(\ell_i \rightarrow \ell_j \gamma) = e m_i \bar{u}_j(p_j) i\sigma^{\mu\nu} q_\nu (A_L P_L + A_R P_R) u_i(p_i) \epsilon_\mu^*(q) \quad (73)$$

¹¹ Especially for $h \rightarrow \mu\tau$ signal, the CMS result gave a 2.4σ hint corresponding to the best-fit branching ratio $\text{Br}(h \rightarrow \mu\tau) = (0.84_{-0.37}^{+0.39})\%$ [86].

FIG. 6: Feynman diagrams contributed to radiative LFV decays $\ell_i \rightarrow \ell_j \gamma$.

in which $P_{L(R)} \equiv (1 \mp \gamma^5)/2$ and q is the momentum of photon. According to Figure 6, there are one-loop and two-loop contributions to these processes where the two-loop diagrams are called Barr-Zee type diagrams [96]¹². For $\tau \rightarrow \mu(e)\gamma$, The analytical expression for left-handed (right-handed) amplitude should be [92–95, 97, 98]¹³

$$\begin{aligned}
A_L^*(A_R) &= A_{L,\text{one-loop}}^*(A_{R,\text{one-loop}}) + A_{L,\text{two-loop}}^*(A_{R,\text{two-loop}}) \\
&= \sum_{\phi} \frac{\sqrt{m_i m_j} c_{\phi,ij} (c_{\phi,ji})}{16\pi^2 v^2} \left(\frac{m_i}{m_h^2} \left(c_{\phi,i} \ln \left(\frac{m_h^2}{m_i^2} \right) - \frac{4}{3} |c_{\phi,i}| \cos(\alpha_{\phi,i}) - \frac{5}{3} i |c_{\phi,i}| \sin(\alpha_{\phi,i}) \right) \right. \\
&\quad + \frac{c_{\phi,V} \alpha}{\pi m_i} \left(\left(3 + \frac{m_{\phi}^2}{2m_W^2} \right) f \left(\frac{m_W^2}{m_{\phi}^2} \right) + \left(\frac{23}{4} - \frac{m_{\phi}^2}{2m_W^2} \right) g \left(\frac{m_W^2}{m_{\phi}^2} \right) + \frac{3}{4} h \left(\frac{m_W^2}{m_{\phi}^2} \right) \right) \\
&\quad \left. - \frac{8\alpha |c_{\phi,t}|}{3\pi m_i} \left(\cos(\alpha_{\phi,t}) f \left(\frac{m_t^2}{m_{\phi}^2} \right) + i \sin(\alpha_{\phi,t}) g \left(\frac{m_t^2}{m_{\phi}^2} \right) \right) \right) \quad (74)
\end{aligned}$$

where $i = \tau, j = e, \mu$, $\alpha_{\phi,f} \equiv \arg(c_{\phi,f})$ and the loop integration functions f, g, h [93, 97] are listed in (B.13)-(B.15) in section B. Numerically the loop contributions with charge Higgs or Z boson inside are both small, thus we ignore them. While for $\mu \rightarrow e\gamma$ decay which means $i = \mu$ and $j = e$, The one-loop contribution should be changed to

$$A_{L,\text{one-loop}}^*(\mu \rightarrow e\gamma) = \sqrt{\frac{m_e}{m_{\mu}}} \sum_{\phi} \frac{m_{\tau}^2 c_{\phi,\tau e} c_{\phi,\mu\tau}}{16\pi^2 m_{\phi}^2 v^2} \left(\ln \left(\frac{m_{\phi}^2}{m_{\tau}^2} \right) - \frac{3}{2} \right) \quad (75)$$

because the loop with τ inside is expected to give larger contribution comparing with the μ

¹² This kind of two-loop diagrams were first used by Barr and Zee to calculate the electric dipole moments for fermion in [96] which would also be discussed later.

¹³ Notice that the analytical formulae for $\ell_i \rightarrow \ell_j \gamma$ decay process in these papers are not consistent with each other. We checked the calculation during finishing our recent paper [92] and confirmed the result by Omura et. al. [94, 95] is correct.

case when adopting the Cheng-Sher ansatz [40]. For A_R we should take $c_{\phi,e\tau}c_{\phi,\tau\mu}$ instead of $c_{\phi,\tau e}c_{\phi,\mu\tau}$ in A_L^* .

Numerically, we take the benchmark points as those in Table I. For $m_\eta = 20\text{GeV}$,

$$\text{Br}(\tau \rightarrow \mu\gamma) \simeq 1.7 \times 10^{-10} (|\xi_{\tau\mu}|^2 + |\xi_{\mu\tau}|^2) |-5.7\xi_{\tau\tau} - 5.4\xi_{tt} + 1.2i|^2; \quad (76)$$

$$\text{Br}(\tau \rightarrow e\gamma) \simeq 8.4 \times 10^{-13} (|\xi_{\tau e}|^2 + |\xi_{e\tau}|^2) |-5.7\xi_{\tau\tau} - 5.4\xi_{tt} + 1.2i|^2. \quad (77)$$

We used $\text{Br}(\tau \rightarrow e\nu_\tau\bar{\nu}_e) = 17.8\%$ and $\text{Br}(\tau \rightarrow \mu\nu_\tau\bar{\nu}_\mu) = 17.4\%$ [29] in the calculations above. For a typical case, $|\xi_{\mu(e)\tau}| \sim |\xi_{\tau\mu(e)}|$, $\xi_{tt} \sim 0.6$ and $\xi_{\tau\tau} \sim 1$, we have $\text{Br}(\tau \rightarrow \mu\gamma) \sim 3 \times 10^{-8}|\xi_{\mu\tau}|^2$, thus the upper limit for $|\xi_{\mu\tau}|$ should be around 1. While for $\text{Br}(\tau \rightarrow e\gamma) \sim 10^{-10}|\xi_{e\tau}|^2$, $|\xi_{e\tau}| \sim \mathcal{O}(10)$ is still allowed. For $m_\eta = 40\text{GeV}$,

$$\text{Br}(\tau \rightarrow \mu\gamma) \simeq 1.7 \times 10^{-10} (|\xi_{\tau\mu}|^2 + |\xi_{\mu\tau}|^2) |-2\xi_{\tau\tau} - 2.5\xi_{tt} - 0.3 + i|^2; \quad (78)$$

$$\text{Br}(\tau \rightarrow e\gamma) \simeq 8.4 \times 10^{-13} (|\xi_{\tau e}|^2 + |\xi_{e\tau}|^2) |-2\xi_{\tau\tau} - 2.5\xi_{tt} - 0.3 + i|^2. \quad (79)$$

Choosing the same parameters as above, $\text{Br}(\tau \rightarrow \mu\gamma) \sim 5 \times 10^{-9}|\xi_{\mu\tau}|^2$ which gives the upper limit of $|\xi_{\mu\tau}|$ to be around 3. While for $\text{Br}(\tau \rightarrow e\gamma) \sim 2 \times 10^{-11}|\xi_{e\tau}|^2$, $|\xi_{e\tau}| \sim \mathcal{O}(10 - 10^2)$ are allowed. In the discussions above, we assumed real $\xi_{tt(\tau\tau)}$. If $\xi_{tt(\tau\tau)}$ were complex, some accidental cancelation would make larger $|\xi_{\mu\tau}|$ possible.

For $\tau \rightarrow \mu\gamma$ decay, it poses a stricter constraint than that from $h \rightarrow \mu\tau$ decay in (68) with $m_\eta \sim (20 - 40)\text{GeV}$. Different from the cases discussed in [92] in which the 125 GeV scalar is the lightest one, in this scenario, the one-loop contribution from (20-40) GeV light scalar would be dominant or at least comparable with the two-loop contributions. At the same time, $h\mu\tau$ vertex is suppressed by s_θ and $t_\beta s_\xi$ to be of $\mathcal{O}(0.1)$. So that in this scenario, $\tau \rightarrow \mu\gamma$ decay gives dominant constraint on the LFV vertex instead of $h \rightarrow \mu\tau$ decay. For $\tau \rightarrow e\gamma$ decay, $|\xi_{e\tau}|$ is constrained to be less than $\mathcal{O}(10 - 10^2)$ which is still away from the expected magnitude by Cheng-Sher ansatz.

Numerically, for $\mu \rightarrow e\gamma$ decay, choosing typically $\xi_{ij} \sim \xi_{ji}$, we have

$$\text{Br}(\mu \rightarrow e\gamma) = 5.7 \times 10^{-9} |-\xi_{e\tau}\xi_{\mu\tau} + \xi_{e\mu}(-0.9\xi_{tt} + 0.2i)|^2, \quad (m_\eta = 20\text{GeV}); \quad (80)$$

$$\text{Br}(\mu \rightarrow e\gamma) = 5.7 \times 10^{-11} |-3.6\xi_{e\tau}\xi_{\mu\tau} + \xi_{e\mu}(-7.7\xi_{tt} + 1.6i)|^2, \quad (m_\eta = 40\text{GeV}). \quad (81)$$

Choosing $|\xi_{tt}| \sim 0.6$ as usual, the three LFV couplings $\xi_{e\mu,e\tau,\mu\tau}$ are strongly correlated between each other. The typical upper limit for $|\xi_{e\mu}|$ and $|\xi_{e\tau}\xi_{\mu\tau}|$ are both of $\mathcal{O}(10^{-2})$ for

$m_\eta \sim (20 - 40)\text{GeV}$. For example, fixing $\xi_{e\tau} = 0$ (or $\xi_{\mu\tau} = 0$),

$$|\xi_{e\mu}| \lesssim (1.4 - 3.3) \times 10^{-2}; \quad (82)$$

while fixing $\xi_{e\mu} = 0$,

$$|\xi_{e\tau}\xi_{\mu\tau}| \lesssim (1.0 - 2.8) \times 10^{-2}. \quad (83)$$

G. Constraints from Electric Dipole Moments

The effective interaction for EDM of a fermion f can be written as [49]

$$\mathcal{L}_{\text{EDM}} = -\frac{i}{2} d_f \bar{f} \sigma^{\mu\nu} \gamma^5 f F_{\mu\nu} \quad (84)$$

which violates both P and CP symmetries. In SM, the only origin of CP-violation is the complex CKM matrix [25, 26] thus the EDM for electron and neutron are generated at four- and three-loop level respectively and they are estimated to be [49]

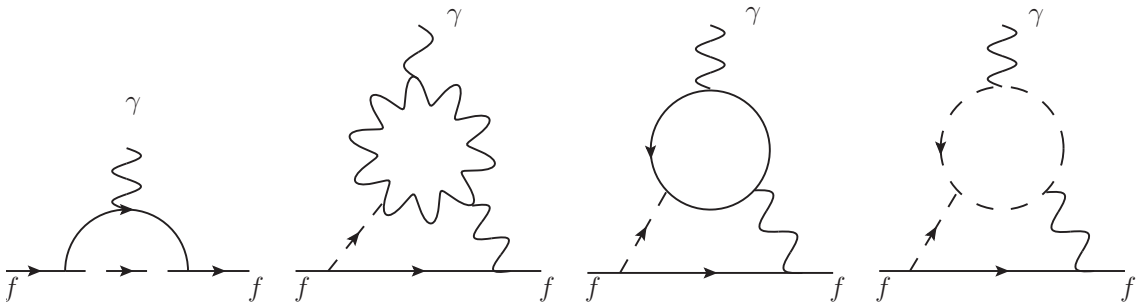
$$d_e \sim 10^{-38} e \cdot \text{cm}, \quad \text{and} \quad d_n \sim 10^{-32} e \cdot \text{cm}. \quad (85)$$

They are still far below the experimental upper limits [47, 48]

$$|d_e| < 8.7 \times 10^{-29} e \cdot \text{cm}, \quad \text{and} \quad |d_n| < 2.9 \times 10^{-26} e \cdot \text{cm}, \quad (86)$$

both at 90% C.L. In BSM with additional origins of CP-violation, the EDM for a fermion might be generated at one- or two-loop level ¹⁴ thus they can be quite larger than those in SM or even reach the sensitivity of recent data.

FIG. 7: Feynman diagrams contributed to EDM for a fermion f .



¹⁴ Non-perturbation effects arising from θ term may also give significant contribution to neutron EDM [99], but we don't include that in this paper.

The EDM for a fermion f can be generated from the Feynman diagrams in Figure 7 if there exist CP-violation in $\phi f \bar{f}$ vertices. The two-loop diagrams are called Barr-Zee diagrams [96]. If there is no CP-violation in flavor-changing vertices, the one loop contributions are proportional to $(m_f/v)^3$ thus they are usually negligible for light fermions. The dominant contributions come from Barr-Zee diagram as [96, 100–102]

$$\frac{d_f}{e} = \sum_{\phi} \frac{2\sqrt{2}\alpha_{\text{em}}G_F Q_f m_f |c_{\phi,f}|}{(4\pi)^3} \left(\sin \alpha_{\phi,f} (c_{\phi,V} \mathcal{J}_1(m_W, m_{\phi}) + g_{\phi,\pm} \mathcal{J}_0(m_{\pm}, m_{\phi})) \right. \\ \left. - \frac{8}{3} |c_{\phi,t}| (\sin \alpha_{\phi,t} \cos \alpha_{\phi,f} \mathcal{J}_{1/2}(m_t, m_{\phi}) + \cos \alpha_{\phi,t} \sin \alpha_{\phi,f} \mathcal{J}'_{1/2}(m_t, m_{\phi})) \right). \quad (87)$$

Here Q_f is the electric charge for fermion f , $\alpha_{\phi,f} \equiv \arg(c_{\phi,f})$, and the $\phi H^+ H^-$ vertex $g_{\phi,\pm} \equiv (1/v)(\partial^3 V / \partial \phi \partial H^+ \partial H^-)$ is defined in (A.10). The first term comes from W^{\pm} loop contribution (the second figure in Figure 7); the second term comes from H^{\pm} loop contribution (the last figure in Figure 7)¹⁵; and the last two terms come from top loop contribution (the third figure in Figure 7). The loop functions \mathcal{J}_i [101] are all listed in section B in (B.16)-(B.19).

For an electron, (87) can fully describe its EDM if we ignore the one-loop contributions. Numerically, we take the benchmark points as those in Table I and fix $|\xi_{tt}| = 0.6$ as usual. Precision measurement by [47] requires strong correlation among parameters to generate the cancelation between different contributions [1, 103]. Define $\alpha_{ij} \equiv \arg(\xi_{ij})$, we show some allowed regions at 90% C.L. in Figure 8-Figure 11 in $\alpha_{ee} - \alpha_{tt}$ plane.

From the figures, We can see for fixing $|\xi_{ee,tt}|$, α_{tt} and α_{ee} have strong negative correlation. In Figure 8 and Figure 9 we both choose $m_{\eta} = 20\text{GeV}$. For $|\xi_{ee}| = 1$, the allowed band is very narrow that $\Delta\alpha \sim 10^{-2}$; while for $|\xi_{ee}| = 0.3$, the allowed band is wider that $\Delta\alpha \sim (3 - 4) \times 10^{-2}$. In Figure 10 and Figure 11 we both choose $m_{\eta} = 40\text{GeV}$. The behaviors are the same as the case $m_{\eta} = 20\text{GeV}$, but the constraints are a bit weaker. For $|\xi_{ee}| = 1$, $\Delta\alpha \sim (1 - 2) \times 10^{-2}$; while for $|\xi_{ee}| = 0.3$, $\Delta\alpha \sim (5 - 7) \times 10^{-2}$. The charged Higgs loops give sub-dominant contributions, thus the final results are not sensitive to $\phi H^+ H^-$ couplings. The location of the allowed regions would shift a little bit for different choices of $\phi H^+ H^-$ couplings.

¹⁵ Numerically the charged Higgs contribution is small comparing with W^{\pm} or top contributions as usual, but it may be comparable with experimental data especially for electron, so it's not negligible like that in radiative LFV decay calculations.

FIG. 8: Constraints in $\alpha_{ee} - \alpha_{tt}$ plane by electron EDM. Fix $m_\eta = 20\text{GeV}$, $|\xi_{tt}| = 0.6$, and $\xi_{ee} = 1$. Yellow regions are allowed at 90% C.L, the same till Figure 11.

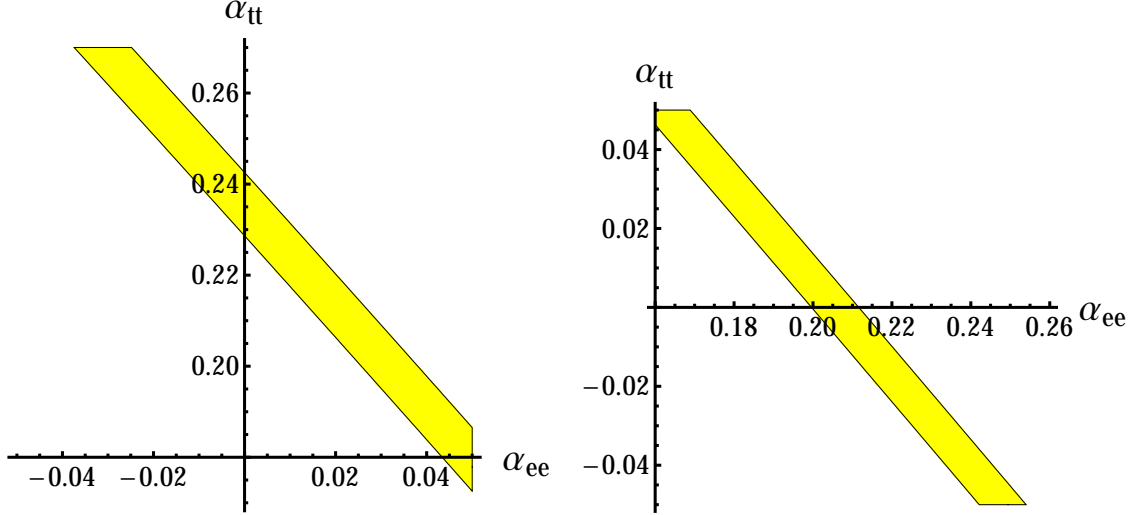
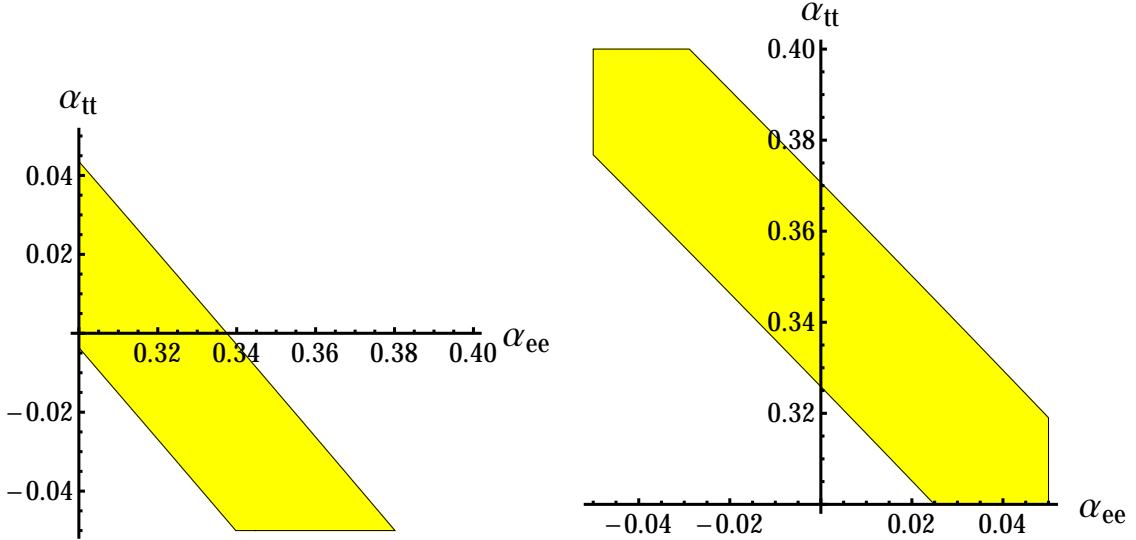


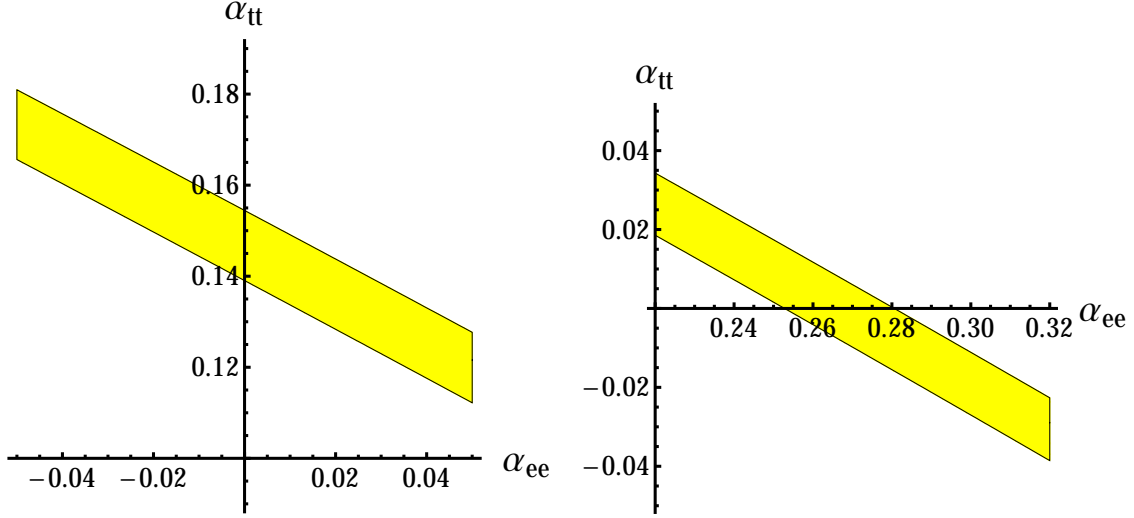
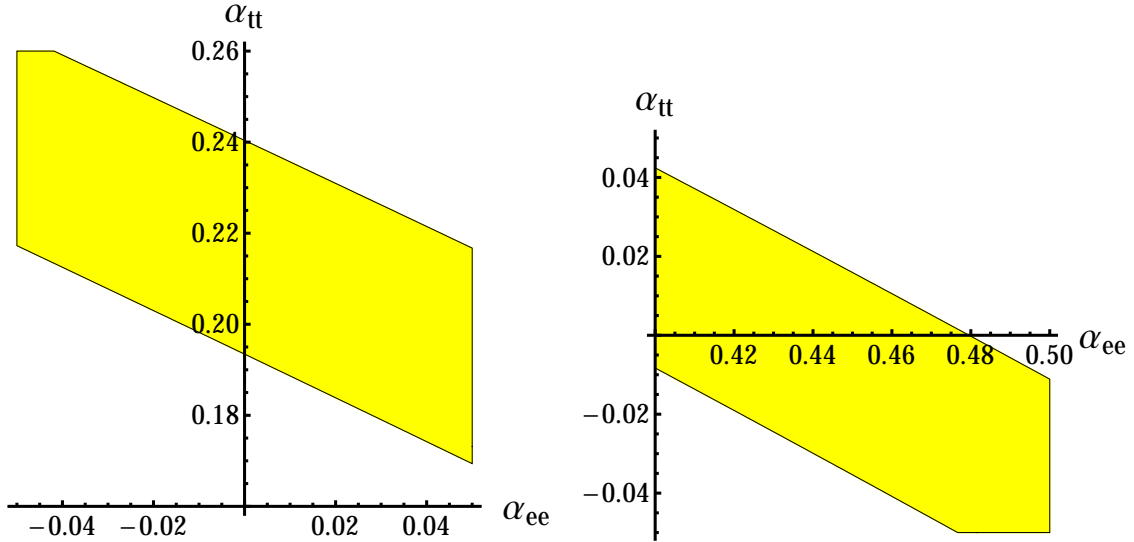
FIG. 9: Constraints in $\alpha_{ee} - \alpha_{tt}$ plane by electron EDM. Fix $m_\eta = 20\text{GeV}$, $|\xi_{tt}| = 0.6$, and $\xi_{ee} = 0.3$.



The one-loop contribution induced by flavor-diagonal interaction, showed as the first figure in Figure 7, is estimated for electron as $|d_e| \sim (em_e m_\tau^2 |c_{\phi, e\tau}|^2 \sin(2\alpha_{\phi, e\tau}) / 16\pi^2 v^2 m_\phi^2) \ln(m_\phi^2/m_e^2) \sim 10^{-32} e \cdot \text{cm}$ which is negligible small. But the flavor-changing vertices should also generate CP-violation effects. If a τ runs in this loop, the one-loop contribution for d_e is [98, 104, 105]

$$\Delta d_e = - \sum_{\phi} \frac{em_e m_\tau^2 |c_{\phi, e\tau}|^2 \sin(2\alpha_{\phi, e\tau})}{16\pi^2 v^2 m_\phi^2} \left(\ln \left(\frac{m_\phi^2}{m_\tau^2} \right) - \frac{3}{2} \right). \quad (88)$$

For $|\xi_{e\tau}| \lesssim 0.1$, one-loop contribution $|d_e| \lesssim 10^{-28} e \cdot \text{cm}$ thus it is negligible comparing with

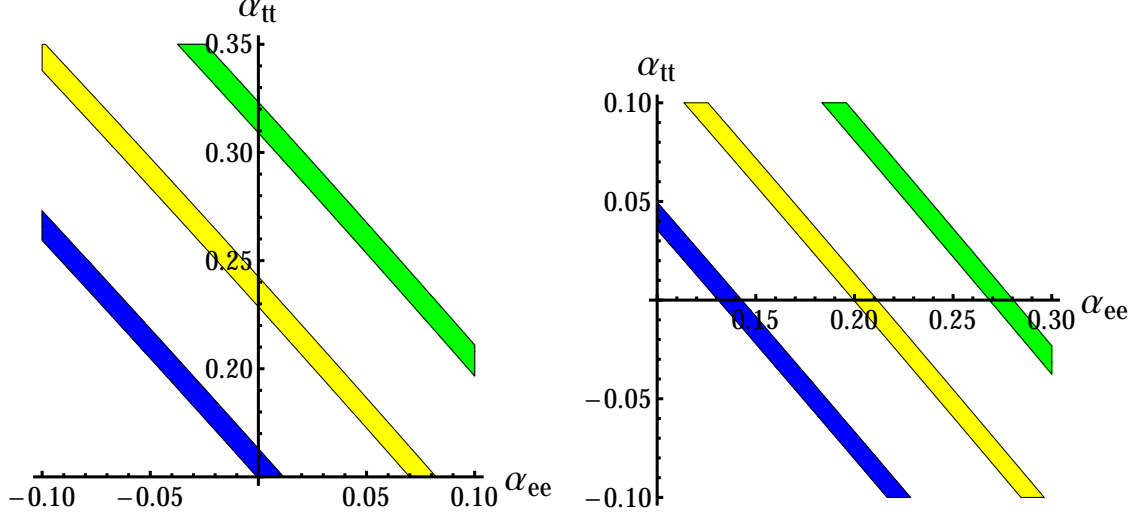
FIG. 10: Constraints in $\alpha_{ee} - \alpha_{tt}$ plane by electron EDM. Fix $m_\eta = 40\text{GeV}$, $|\xi_{tt}| = 0.6$, and $\xi_{ee} = 1$.FIG. 11: Constraints in $\alpha_{ee} - \alpha_{tt}$ plane by electron EDM. Fix $m_\eta = 40\text{GeV}$, $|\xi_{tt}| = 0.6$, and $\xi_{ee} = 0.3$.

the recent experimental sensitivity [47]. While if $|\xi_{e\tau}|$ are larger, for example, we can take $|\xi_{e\tau}| \sim \mathcal{O}(1)$ ¹⁶, one-loop contribution to $|d_e|$ would reach $\mathcal{O}(10^{-27} - 10^{-26})e \cdot \text{cm}$. In this case, the allowed region would be modified a little bit. As an example, for the parameters in Figure 8, we show the allowed region before and after adding the one-loop contribution $\Delta d_e = \pm 10^{-27}e \cdot \text{cm}$ in Figure 12.

The neutron EDM contains four types of contribution [49], including quark EDM d_q ,

¹⁶ Which means $|\xi_{\mu\tau}| \lesssim \mathcal{O}(10^{-2})$ according to (83).

FIG. 12: Constraints in $\alpha_{ee} - \alpha_{tt}$ plane by electron EDM. Fix $m_\eta = 20\text{GeV}$, $|\xi_{tt}| = 0.6$, and $\xi_{ee} = 1$. Yellow regions are allowed for the case without one-loop contribution. Green regions are for one-loop contribution $\Delta d_e = +10^{-27}e \cdot \text{cm}$ while blue regions are for one-loop contribution $\Delta d_e = -10^{-27}e \cdot \text{cm}$.



quark color EDM (CEDM) \tilde{d}_q , Weinberg operator [106, 107] w , and strong CP term [99] which would not be discussed in this paper. Thus [49, 100]

$$\frac{d_n}{e} \simeq 1.4 \left(\frac{d_d}{e} - 0.25 \frac{d_u}{e} \right) + 1.1 \left(\tilde{d}_d + 0.5 \tilde{d}_u \right) + (22\text{MeV})w. \quad (89)$$

Ignore the CP-violation effects in flavor-changing vertices now, the EDM for u and d quarks are just those in (87) which come from the Barr-Zee type contributions. And the CEDM from Barr-Zee diagrams are given by [96, 100]

$$\begin{aligned} \tilde{d}_q = & - \sum_{\phi} \frac{2\sqrt{2}G_F\alpha_s m_q |c_{\phi,t}c_{\phi,q}|}{(4\pi)^3} \\ & (\sin \alpha_{\phi,t} \cos \alpha_{\phi,q} \mathcal{J}_{1/2}(m_t, m_\phi) + \cos \alpha_{\phi,t} \sin \alpha_{\phi,q} \mathcal{J}'_{1/2}(m_t, m_\phi)) \end{aligned} \quad (90)$$

where the loop functions are the same as those in (87). The contribution from Weinberg operator is [100, 106, 107]

$$w = \sum_{\phi} \frac{\sqrt{2}G_F g_s \alpha_s |c_{\phi,t}|^2}{4 \cdot (4\pi)^3} \sin \alpha_{\phi,t} \cos \alpha_{\phi,t} \mathcal{K} \left(\frac{m_t^2}{m_\phi^2} \right) \quad (91)$$

where the loop function \mathcal{K} is listed in (B.22) in section B. Including also the running effects

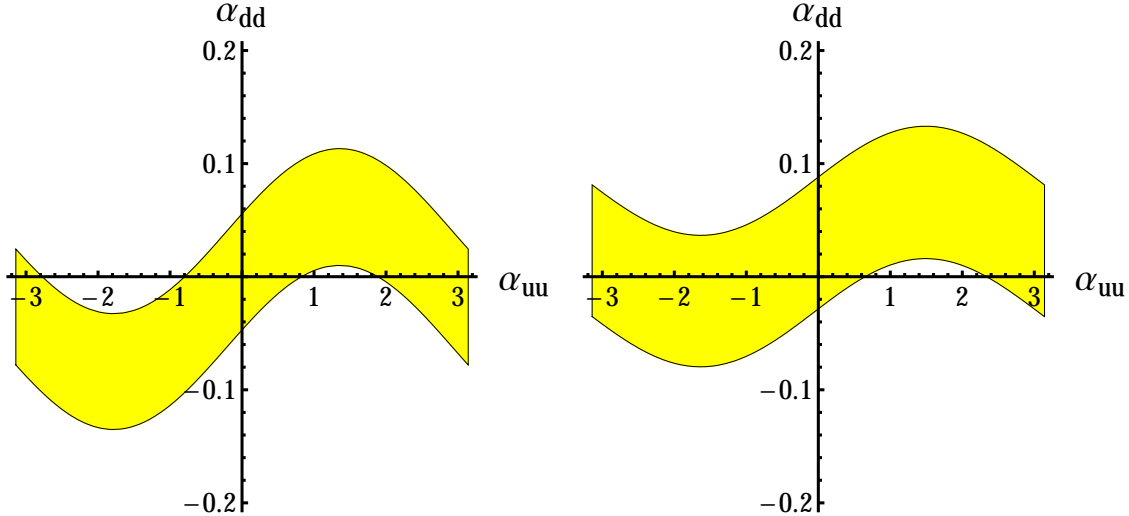
for these operators (see the appendices in [100]),

$$\frac{d_n}{e} \simeq \frac{m_d(\mu_H)}{m_d(\mu_W)} \left(0.63 \frac{d_d(\mu_W)}{e} + 0.73 \tilde{d}_d(\mu_W) \right) + \frac{m_u(\mu_H)}{m_u(\mu_W)} \left(-0.16 \frac{d_u(\mu_W)}{e} + 0.19 \tilde{d}_u(\mu_W) \right) + (8.8 \text{MeV} + 0.17 m_d(\mu_H) + 0.08 m_u(\mu_H)) w(\mu_W). \quad (92)$$

Here μ_H is the hadron scale and μ_W is the electro-weak scale, $\alpha_s(\mu_W) \approx 0.11$ [108], and $m_d(\mu_H) \approx 4.8 \text{MeV}$, $m_u(\mu_H) \approx 2.3 \text{MeV}$ [29]. $d_q(\mu_W)$, $\tilde{d}_q(\mu_W)$, and $w(\mu_W)$ are all calculated at electro-weak scale.

Numerically, we use the benchmark points the same as above. Fixing $|\xi_{uu}| = |\xi_{dd}| = 1$, $|\xi_{tt}| = 0.6$, and $\alpha_{tt} = 0$. For $m_\eta = 20 \text{GeV}$ and $m_\eta = 40 \text{GeV}$, we show the allowed regions in $\alpha_{uu} - \alpha_{dd}$ plane in Figure 13. There exist cancelation between different contributions as well. From the figures, we can see α_{uu} is almost free, and α_{dd} is constrained in a narrow band. For both cases, $\alpha_{uu} = \alpha_{dd} = 0$ is inside the allowed region, and $\Delta\alpha_{dd} \sim 0.1$. The cancelation behavior is not sensitive to m_η . It is also a strict constraint from neutron EDM, but not so strict as that from electron EDM.

FIG. 13: Allowed region on $\alpha_{uu} - \alpha_{dd}$ plane with constraint from neutron EDM. We fix $|\xi_{uu}| = |\xi_{dd}| = 1$, $|\xi_{tt}| = 0.6$, and $\alpha_{tt} = 0$. The left figure is for $m_\eta = 20 \text{GeV}$ and the right one is for $m_\eta = 40 \text{GeV}$. All other benchmark points are the same as above. Yellow regions are allowed at 90% C.L.



Next, consider the contributions from flavor-changing vertices. Strict constraints from meson mixing (see the text in section III D) require that the contributions for d_n from $bd\phi$, $sd\phi$, and $uc\phi$ vertices should be less than $\mathcal{O}(10^{-30})e \cdot \text{cm}$, thus they can be ignorable. But

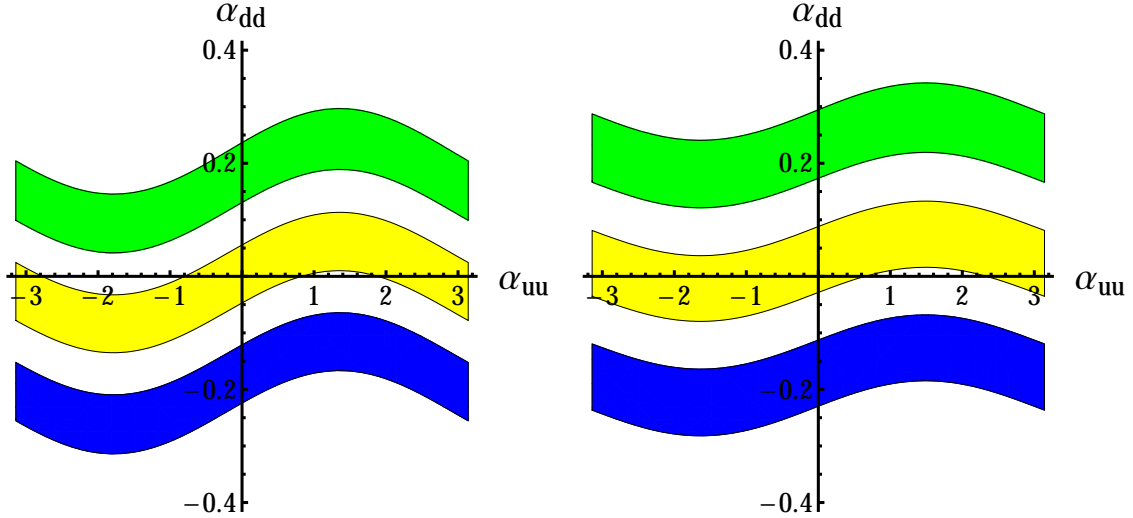
CP-violation in $tu\phi$ vertex would give larger contribution to d_u and \tilde{d}_u [98, 104, 105] through the one-loop diagram as the left figure in Figure 7,

$$\frac{\Delta d_u}{e} = \sum_{\phi} \frac{m_u |c_{\phi,tu}|^2 \sin(2\alpha_{\phi,tu})}{24\pi^2 v^2} \mathcal{P}_1 \left(\frac{m_t^2}{m_{\phi}^2} \right); \quad (93)$$

$$\Delta \tilde{d}_u = \sum_{\phi} \frac{m_u |c_{\phi,tu}|^2 \sin(2\alpha_{\phi,tu})}{16\pi^2 v^2} \mathcal{P}_1 \left(\frac{m_t^2}{m_{\phi}^2} \right). \quad (94)$$

The loop function $\mathcal{P}_1(x)$ is listed in (B.23) in section B. For $|\xi_{tu}| \sim 1$, the additional contribution to neutron EDM can reach $\Delta d_n \sim \mathcal{O}(10^{-26} - 10^{-25})e \cdot \text{cm}$, which would change the cancelation behavior and shift the allowed region a little bit. In Figure 14, we show the allowed region before and after adding the one-loop contribution $\Delta d_n = \pm 10^{-25}e \cdot \text{cm}$. The

FIG. 14: Allowed region by the constraint from neutron EDM. Benchmark points are the same as above in Figure 13. Yellow regions are allowed for the case without one-loop contribution. Green regions are for one-loop contribution $\Delta d_n = +10^{-25}e \cdot \text{cm}$ while blue regions are for one-loop contribution $\Delta d_n = -10^{-25}e \cdot \text{cm}$.



case $|\Delta d_n| \gtrsim 6 \times 10^{-25}e \cdot \text{cm}$ is excluded for this benchmark points choice because enough cancelation between different contributions cannot be generated.

H. Constraints from B Meson Rare Decays

The leptonic decay $B_{(s)}^0 \rightarrow \mu^+ \mu^-$ was measured by CMS and LHCb collaborations and the results [109–111] are listed in Table IV together with their SM predictions [112, 113]. Both

TABLE IV: Recent experimental and theoretical results for $B_{(s)}^0 \rightarrow \mu^+ \mu^-$ decay branching ratios.

Result	$\text{Br}(B_s^0 \rightarrow \mu^+ \mu^-)$	$\text{Br}(B^0 \rightarrow \mu^+ \mu^-)$
CMS	$(2.8_{-0.9}^{+1.1}) \times 10^{-9}$	$(4.4_{-1.9}^{+2.2}) \times 10^{-10}$
LHCb	$(2.7_{-0.9}^{+1.1}) \times 10^{-9}$	$(3.3_{-2.1}^{+2.4}) \times 10^{-10}$
Combined	$(2.8_{-0.6}^{+0.7}) \times 10^{-9}$	$(3.9_{-1.4}^{+1.6}) \times 10^{-10}$
SM Prediction	$(3.65 \pm 0.23) \times 10^{-9}$	$(1.06 \pm 0.09) \times 10^{-10}$

measurements are almost consistent with SM predictions¹⁷, thus new physics contributions would be limited.

The tree level contributions to $B_{(s)}^0 \rightarrow \mu^+ \mu^-$ is negligible [1] due to the constraints from B meson mixing. Here we consider the charged Higgs contribution only. In this scenario, $m_{\pm} \sim v$ is favored as above. For $|\xi_{bb,dd,\ell\ell}| \sim \mathcal{O}(1)$, the modified branching ratio for $B_{(s)}^0 \rightarrow \mu^+ \mu^-$ should be [114]

$$\frac{\text{Br}(B_{(s)}^0 \rightarrow \mu^+ \mu^-)}{\text{Br}_{\text{SM}}(B_{(s)}^0 \rightarrow \mu^+ \mu^-)} = \left(1 - \frac{|\xi_{tt}|^2}{\eta} \frac{\mathcal{Y}_{2\text{HDM}}(m_t^2/m_W^2, m_{\pm}^2/m_W^2)}{\mathcal{Y}_{\text{SM}}(m_t^2/m_W^2)} \right)^2 \quad (95)$$

where $\eta = 0.987$ is the QCD and electro-weak correlation factor and the loop functions \mathcal{Y}_i are listed in (B.25)-(B.26) in section B. Numerically, consider $B_s^0 \rightarrow \mu^+ \mu^-$, both CMS and LHCb results give

$$|\xi_{tt}| \lesssim (0.7 - 0.8) \quad (96)$$

at 95% C.L. which is near the constraint by B meson mixing in (58). For $B_d^0 \rightarrow \mu^+ \mu^-$ decay, these regions are also allowed at 95% C.L. by both CMS and LHCb results¹⁸.

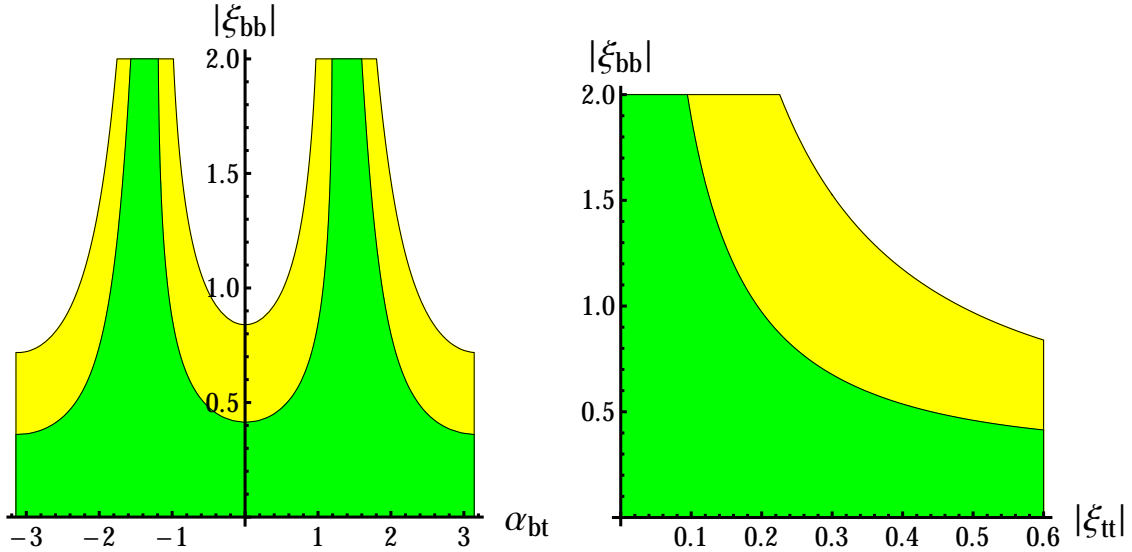
The world averaged value for B radiative decay branching ratio reads $\text{Br}_{\text{ave}}(\bar{B} \rightarrow X_s \gamma) = (3.43 \pm 0.22) \times 10^{-4}$ [67] which is consistent with its SM prediction $\text{Br}_{\text{SM}}(\bar{B} \rightarrow X_s \gamma) = (3.36 \pm 0.23) \times 10^{-4}$ [115]. In 2HDM, according to (25), a charged Higgs boson can also run in the loop instead of W^{\pm} for the radiative decay process thus the branching ratio can be modified. In type II 2HDM, the charged Higgs mass is constrained to be larger than

¹⁷ The CMS result for $\text{Br}(B^0 \rightarrow \mu^+ \mu^-)$ has a deviation from SM prediction at about 2σ level. The same thing happens to the combined result for $\text{Br}(B^0 \rightarrow \mu^+ \mu^-)$.

¹⁸ If considering the combined result, $|\xi_{tt}| \lesssim (0.5 - 0.6)$ is still allowed by data due to $B_s^0 \rightarrow \mu^+ \mu^-$ which is a bit stricter than that in (58). For $B_d^0 \rightarrow \mu^+ \mu^-$, we also need $|\xi_{tt}| \gtrsim (0.2 - 0.3)$ at 95% C.L. because the combined deviation between $\text{Br}(B^0 \rightarrow \mu^+ \mu^-)$ and its SM prediction is a bit larger than 2σ .

about 410 GeV [116]¹⁹ at 95% C.L. But in a general 2HDM, a lighter charged Higgs boson may be allowed [1]. Different from leptonic decay, the radiative decay branching ratio is sensitive to not only m_{\pm} and ξ_{tt} , but also ξ_{bb} . For a general case, $\alpha_{bt} \equiv \arg(\xi_{bb}/\xi_{tt})$ is also a free parameter. Based on [116] and the mathematica code, we plot the constraints on these parameters in Figure 15 and Figure 16, fixing $m_{\pm} = 200\text{GeV}$ and $m_{\pm} = 300\text{GeV}$ respectively. From the figures, we can see for $|\xi_{tt}| = 0.6$, for most α_{bt} choice, we have

FIG. 15: Constraints by $\text{Br}(\bar{B} \rightarrow X_s \gamma)$ fixing $m_{\pm} = 200\text{GeV}$. In the left figure, we take $|\xi_{tt}| = 0.6$ and plot the allowed region in $|\xi_{bb}| - \alpha_{bt}$ plane. In the right figure, we take $\alpha_{bt} = 0$ and plot the allowed region in $|\xi_{bb}| - |\xi_{tt}|$ plane. In both figures, green regions are allowed at 68% C.L. and the yellow regions are allowed at 95% C.L.



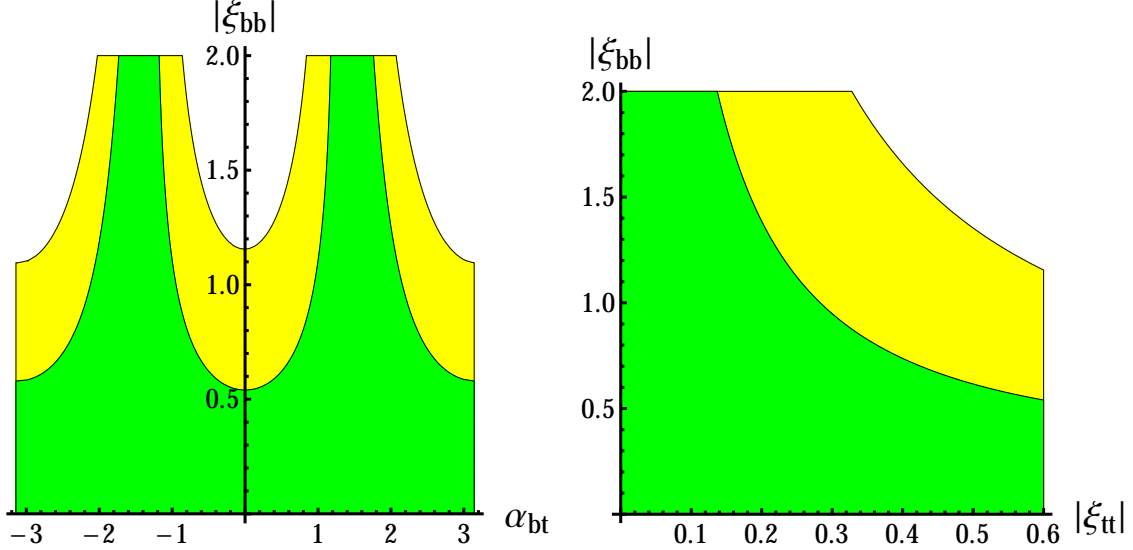
$|\xi_{bb}| \lesssim 1$; but for some α_{bt} choice, a larger $|\xi_{bb}|$ is also allowed. While for fixed α_{bt} , there is also larger allowed region in $|\xi_{bb}| - |\xi_{tt}|$ plane. The constraint is not so strict as that for type II 2HDM because more parameters are free, just like the case in [1].

IV. PREDICTIONS AND FUTURE TESTS FOR THIS SCENARIO

We have discussed all the constraints on the Lee model in an alternative scenario which is weakly-coupled. As shown above, it is still not excluded by experimental results. Comparing

¹⁹ This value is different from the data in the text of [116] because the SM prediction result was updated in [115] recently.

FIG. 16: Constraints by $\text{Br}(\bar{B} \rightarrow X_s \gamma)$ fixing $m_{\pm} = 300\text{GeV}$. All other sets are the same as those in Figure 15.



with the scenario in [1], the particle spectrum are the same. But in this scenario, all the scalars are required to have their mass around electro-weak scale or lighter. Especially, the lightest scalar is required to have its mass $m_\eta \sim \mathcal{O}(10\text{GeV})$ which means new physics is hidden in the scale lower than electro-weak scale. That's different from the scenario in [1] in which new physics would appear at $\mathcal{O}(\text{TeV})$ or higher scale.

In this scenario, the couplings of the 125 GeV Higgs boson is SM-like, but other particles are not decoupled thus they would face future tests at colliders. A lighter scalar can also appear through Higgs decay channels $h \rightarrow Z\eta, \eta\eta$ which are worth to search. Different scalars may also be produced associated with each other or with heavy quark (pair). $h \rightarrow Z\eta, \eta\eta$ rare decays would also be constrained by Higgs signal strengths which would be measured precisely in the future. Experiments on flavor changing processes and EDM measurements would also help to confirm or exclude this scenario indirectly.

A. Direct Searches for Extra Scalars at Future Colliders

The key prediction of this scenario (weakly-coupled Lee model) is a light particle η with its mass of $\mathcal{O}(10\text{GeV})$. It should be a CP-mixing state with pseudoscalar component dominant. Its low mass is correlated with the smallness of CP-violation. At LHC, it certainly can be produced through gluon fusion or $b\bar{b}$ fusion with large cross section, but such a light particle

would be hidden below the huge QCD background [13], thus it is difficult to be discovered. At LHC with $\sqrt{s} = (13 - 14)\text{TeV}$, η can also be produced in associated with top quark pair with a cross section of $\mathcal{O}(0.1)\text{pb}$ [117]. According to [117], at LHC with $\sqrt{s} = 14\text{TeV}$ and 3ab^{-1} luminosity, for $m_\eta \sim (20 - 40)\text{GeV}$, the constraint $|\xi_{tt}| \lesssim (0.34 - 0.54)$ at 95% C.L. would be achieved assuming no positive results. It would be stricter than all the recent constraints obtained from indirect processes. On the other hand, for $m_\eta \sim (30 - 40)\text{GeV}$, the benchmark case $|\xi_{tt}| = 0.6$ would be discovered at more than 5σ .

η can also appear as the decay final state of other scalars, such as $h, H \rightarrow \eta\eta, Z\eta$, etc. We will study the cascade decay channels in details in the future. LHeC [118, 119] would be a better collider in searching for the exotic Higgs decays [120]. At future e^+e^- colliders [121–124], η is also possible to be discovered through Higgs rare decay processes, such as $e^+e^- \rightarrow Zh(\rightarrow \eta\eta)$. At the Higgs factories with $\sqrt{s} \sim (240 - 250)\text{GeV}$ like CEPC [123] or TLEP [121], this process can be discovered at 5σ with 5ab^{-1} luminosity if $\text{Br}(h \rightarrow \eta\eta) > 10^{-3}$ [123]. η can also be produced in associated with Z or h at CEPC or TLEP. With a roughly estimation comparing with LEP results [50–52, 65] we used in section III A, using $\mathcal{O}(10^2 - 10^3)\text{fb}^{-1}$ luminosity, the sensitivity to $c_{\eta,V}$ and $c_{h\eta}(=c_{H,V})$ would improve at least an order. At e^+e^- colliders with $\sqrt{s} > m_\eta + m_H$, it is possible to produce η and H through $e^+e^- \rightarrow \eta H$ ²⁰. It's worth noting that under weak-coupling assumption, m_H should be around the electro-weak scale, and $c_{\eta H} = c_h \sim 1$ would never be suppressed, thus this is also a key process to confirm or exclude this scenario at future e^+e^- colliders.

For the heavy Higgs boson H , it is required to have a mass around v thus it is possible to be discovered at LHC [125]. For $m_H \sim (200 - 300)\text{GeV}$, choose $|\xi_{tt}| = 0.6$ and $c_{H,V} = 0.3$ we take above, the cross section $\sigma(pp \rightarrow H \rightarrow ZZ) \sim (120 - 200)\text{fb}$ according to [126] at future LHC with $\sqrt{s} = 14\text{TeV}$. It is larger than the 5σ discovery threshold $(50 - 100)\text{fb}$ using 3ab^{-1} luminosity [125], thus it would be easily discovered. While if no signal evidence were found, according to [125], the 95% C.L. limit for $\sigma(pp \rightarrow H \rightarrow ZZ)$ would be $(20 - 40)\text{fb}$ for the mass region $m_H \sim (200 - 300)\text{GeV}$. Since the dominant production channel for H is gluon fusion, this result means the future LHC would be able to set the constraint

$$|\xi_{tt}|c_{H,V} \lesssim 0.08 \quad (97)$$

at 95% C.L. if no evidence for this channel were found.

²⁰ If $m_H \sim 200\text{GeV}$, Higgs factory mentioned above is also allowed for this process.

Through the oblique parameter constraints, the charged Higgs mass is around v in this scenario. It must face the direct searches at LHC or e^+e^- colliders. At LHC, it can be produced through $gb \rightarrow tH^-$ associated production [127] which was used to search for the charged Higgs boson in [57]. For a light charged higgs with $m_{\pm} \sim (200 - 300)\text{GeV}$, for $|\xi_{tt}| \sim 0.6$ and $|\xi_{bb}| \sim \mathcal{O}(1)$, it would be discovered at LHC with $\sqrt{s} = (13 - 14)\text{TeV}$ and 300fb^{-1} luminosity; and the polarization of top quark would also be useful to test the chiral structure in tbH^- vertex [128–130]. At e^+e^- colliders with $\sqrt{s} \gtrsim 500\text{GeV}$, we can discover the charged Higgs boson through $e^+e^- \rightarrow H^+H^-$ process [131, 132]. This process would not be suppressed as well, thus it is useful to confirm or exclude this scenario. In Table V and Table VI we summarize the mentioned channel above which would be useful to test this scenario in the future [117, 123, 125–133].

TABLE V: Examples for main processes which would be useful to test this scenario at future pp collider. “*” means we will study this process in details in the future. In this table, all masses are chosen as: $m_{\eta} = 40\text{GeV}$, $m_h = 125\text{GeV}$, and $m_H = m_{\pm} = 300\text{GeV}$ as an example. The benchmark points listed here for collider or model parameters are possible choices but not the only choice for the corresponding processes.

Collider	Process	\sqrt{s} (TeV)	Couplings and/or Branching Ratios	Cross Section (pb)	Implications
LHC	$pp \rightarrow t\bar{t}\eta$	14	$ \xi_{tt} = 0.6$	0.18	Over 5σ discovery with 3ab^{-1} luminosity assuming $\text{Br}_{\eta \rightarrow b\bar{b}} = 1$.
LHC	$pp \rightarrow H(ZZ)$	14	$ \xi_{tt} = 0.6$ $\text{Br}_{H \rightarrow ZZ} = 3\%$	0.12	Over 5σ discovery with 3ab^{-1} luminosity.
LHC	$pp \rightarrow H(Z\eta, \eta\eta)$	14	$c_{H\eta} = c_{h,V} = 0.95$, $ \xi_{tt} = 0.6, g_{H\eta\eta} \sim 1$	$4 \times \text{Br}_{H \rightarrow Z\eta, \eta\eta}$	*To be studied.
LHC	$pp(bg) \rightarrow tH^-(\bar{t}b)$	14	$ \xi_{tt} = 0.6, \xi_{bb} \lesssim 1$ $\text{Br}_{H^- \rightarrow \bar{t}b} = 1$	0.6	5σ discovery with $\mathcal{O}(10^2)\text{fb}^{-1}$ luminosity.

If all the three neutral scalars and their couplings to VV were discovered in the future, the associated productions for any two scalars are important to confirm CP-violation in Higgs sector as well. Since in a general model, if no CP-violation exists in scalar sector,

TABLE VI: Examples for main processes which would be useful to test this scenario at future e^+e^- colliders. “*” means we will study this process in details in the future. In this table, all masses are chosen as: $m_\eta = 40\text{GeV}$, $m_h = 125\text{GeV}$, and $m_H = m_\pm = 300\text{GeV}$ as an example. The benchmark points listed here for collider or model parameters are possible choices but not the only choice for the corresponding processes.

Collider	Process	\sqrt{s} (TeV)	Couplings and/or Branching Ratios	Cross Section (pb)	Implications
CEPC	$e^+e^- \rightarrow Z\eta$	0.25	$c_{\eta,V} = 0.1$	4.4×10^{-3}	*Sensitivity to $c_{\eta,V}$ would reach $\mathcal{O}(10^{-2})$ with 5ab^{-1} luminosity.
CEPC	$e^+e^- \rightarrow h\eta$	0.25	$c_{h\eta} = c_{H,V} = 0.3$	7.3×10^{-3}	*Sensitivity to $c_{H,V}$ would reach $\mathcal{O}(10^{-2})$ with 5ab^{-1} luminosity.
CEPC	$e^+e^- \rightarrow Zh(\eta\eta)$	0.25	$c_{h,V} = 0.95$ $\text{Br}_{\eta \rightarrow b\bar{b}} = 1$	$0.19 \times \text{Br}_{h \rightarrow \eta\eta}$	5σ discovery with 5ab^{-1} luminosity if $\text{Br}_{h \rightarrow \eta\eta} > 10^{-3}$
ILC	$e^+e^- \rightarrow H\eta$	0.5	$c_{h,V} = 0.95$	1×10^{-2}	*To be studied.
ILC	$e^+e^- \rightarrow H^+H^-$	0.8	$\text{Br}_{H^- \rightarrow b\bar{b}} = 1$	1.4×10^{-2}	Cross section can be measured to 9% with 1ab^{-1} luminosity.

all the three discovered neutral scalars should be CP-even²¹ thus there would be no direct $h_i h_j Z$ vertices. The $e^+e^- \rightarrow h_i h_j$ process would be loop induced in this case thus the cross section would be highly suppressed. If the cross sections showed there exists tree level $h_i h_j Z$ vertices²², the scalars must contain different CP components thus we would be able to confirm CP-violation in scalar sector [133]²³.

²¹ This case cannot appear in 2HDM, there must be additional scalar degree of freedoms, such as another Higgs doublet.

²² For example, if the cross sections satisfied the relations in (A.15).

²³ Notice this is a model-independent method to confirm CP-violation in scalar sector. But it cannot be used to exclude CP-violation in scalar sector, because in some models, there are no direct $h_i h_j Z$ vertices even CP-violation exists in scalar sector.

B. Future Measurements on 125 GeV Higgs Boson

In this scenario, the couplings between 125 GeV Higgs boson h and SM particles should be SM-like. Exotic decay channels $h \rightarrow \eta\eta$ or $Z\eta$ make the total width of h larger, which would also affect other decay channels of h . In the future, LHC can measure the signal strengths $h \rightarrow \gamma\gamma, ZZ^*, WW^*, b\bar{b}, \tau^+\tau^-$ to the precision $(11-14)\%$ with 300fb^{-1} luminosity, and $(7-8)\%$ with 3ab^{-1} luminosity [134, 135].

In this scenario, the modification of Higgs couplings to fermions or gauge bosons should be at percent level, for some cases it can reach 10%. Under this assumption, if the future signal strengths were all consistent with SM prediction, we perform a global-fit and estimate that at least $\Gamma_{\text{exo}} \lesssim (0.4-0.6)\text{MeV}$ (or equivalently $\text{Br}_{\text{exo}} \lesssim (10-15)\%$) would still be allowed in this scenario. The direct measurements at future LHC cannot reach the sensitivity to test the modification of Higgs signal strengths from those in SM.

At future e^+e^- colliders, such as the Higgs factories CEPC [123] or ILC [124, 131] with $\sqrt{s} \sim (240-250)\text{GeV}$, to the luminosity of $\mathcal{O}(\text{ab}^{-1})$, all the channels mentioned above together with Higgs total width can be measured to percent level or even better. For $c_{h,V} \sim 0.95$, $\Delta\sigma_{Zh}/\sigma_{Zh} \sim 10\%$ which can be measured with $\mathcal{O}(0.1\text{ab}^{-1})$ luminosity. The precision measurements on $h \rightarrow b\bar{b}, \tau^+\tau^-$ are also helpful to distinguish this scenario from SM. If no deviations were found, $|\xi_{bb,\tau\tau}|$ would be constrained to $\mathcal{O}(1)$. For $h \rightarrow gg$ decay, it is sensitive to both $|c_{h,t}|$ and $\alpha_{h,t}$. The exotic decays $h \rightarrow \eta\eta, Z\eta$ would also be discovered or further constrained at Higgs factory.

CP-violation is a main feather in Lee model, for example, the $hf\bar{f}$ couplings would contain CP-violation. For τ lepton and top quark, the decay distribution would include its polarization information thus it is possible to test the CP-violation effects in $ht\bar{t}$ and $h\tau^+\tau^-$ vertices [131]. At LHC with $\sqrt{s} = 13\text{TeV}$ and 3ab^{-1} luminosity, using $h \rightarrow \tau^+\tau^-$ decay mode, it is possible to measure $\alpha_{h,\tau}$ to the sensitivity $\Delta\alpha_{h,\tau} \sim 4^\circ$ with the help of final states distribution in τ decay [136]; while at e^+e^- collider, with $\sqrt{s} = 250\text{GeV}$ and 1ab^{-1} luminosity, this sensitivity would reach $\Delta\alpha_{h,\tau} \sim 2.8^\circ$ [137]; which are both enough to test this scenario. For $ht\bar{t}$ coupling, we can use $e^+e^- \rightarrow t\bar{t}h$ associated production to test $\alpha_{h,t}$ [105, 131, 138], with $\sqrt{s} > 2m_t + m_h \sim 470\text{GeV}$.

C. EDM for Third Generation Fermions

As mentioned above, the polarization of a τ lepton or top quark can affect on the distribution of its decay final states. With this property, it may be possible to test their anomalous electro-weak couplings including EDM. For a heavy fermion such as τ, b, t , if one-loop contribution to CP-violation (see Figure 7) exists, the Barr-Zee type contribution would be ignorable. The one-loop contribution reads [104, 105]

$$d_f = \frac{Q_f m_f^3}{16\pi^2 v^2} \sum_{\phi} \frac{|c_{\phi,f}|^2 \sin(2\alpha_{\phi,f})}{m_{\phi}^2} \mathcal{P}_2 \left(\frac{m_f^2}{m_{\phi}^2} \right) \quad (98)$$

where the loop function $\mathcal{P}_2(x)$ is listed in (B.24) in section B.

For a τ lepton,

$$|d_{\tau}| \lesssim \frac{m_{\tau}^3 |\xi_{\tau\tau}|^2}{16\pi^2 v^2 m_{\eta}^2} \left(\ln \left(\frac{m_{\eta}^2}{m_{\tau}^2} \right) - \frac{3}{2} \right) \sim 10^{-22} |\xi_{\tau\tau}|^2 e \cdot \text{cm}. \quad (99)$$

If $|\xi_{\tau\tau}| \sim 1$, it is still far away from the future sensitivity of τ EDM, around $\mathcal{O}(10^{-19} e \cdot \text{cm})$, given by SuperB [139, 140] with $\sqrt{s} = m_{\Upsilon(4S)}$ and $(50 - 75) \text{ab}^{-1}$ luminosity or CEPC [123] with $\sqrt{s} = 240 \text{GeV}$ and 5ab^{-1} luminosity. But for a top quark, it can be larger due to its large mass. With the benchmark points in Table I, for $|\xi_{tt}| = 0.6$ and $m_{\eta} \sim (20 - 40) \text{GeV}$, $|d_t|$ can reach $\mathcal{O}(10^{-19} - 10^{-18}) e \cdot \text{cm}$ which would be possibly tested at future e^+e^- colliders with $\mathcal{O}(\text{ab}^{-1})$ luminosity [105, 141].

D. Future Tests in Flavor Physics

At future SuperB with $(50 - 75) \text{ab}^{-1}$ luminosity [139, 140] and LHCb with 50fb^{-1} luminosity [142] experiments, for $B_{(s)}^0 - \bar{B}_{(s)}^0$ mixing, the sensitivity to $\Delta_{B(B_s)}$ in (52) would reach $(3 - 7) \times 10^{-2}$ given by [74]. With these sensitivity, if no deviations in B meson mixing were found, it would require $|\xi_{tt}| \lesssim (0.2 - 0.3)$ at 95% C.L. While the benchmark point we choose in the text above, $|\xi_{tt}| \sim 0.6$, would lead to at least a 5σ deviation from SM prediction in B meson mixing results.

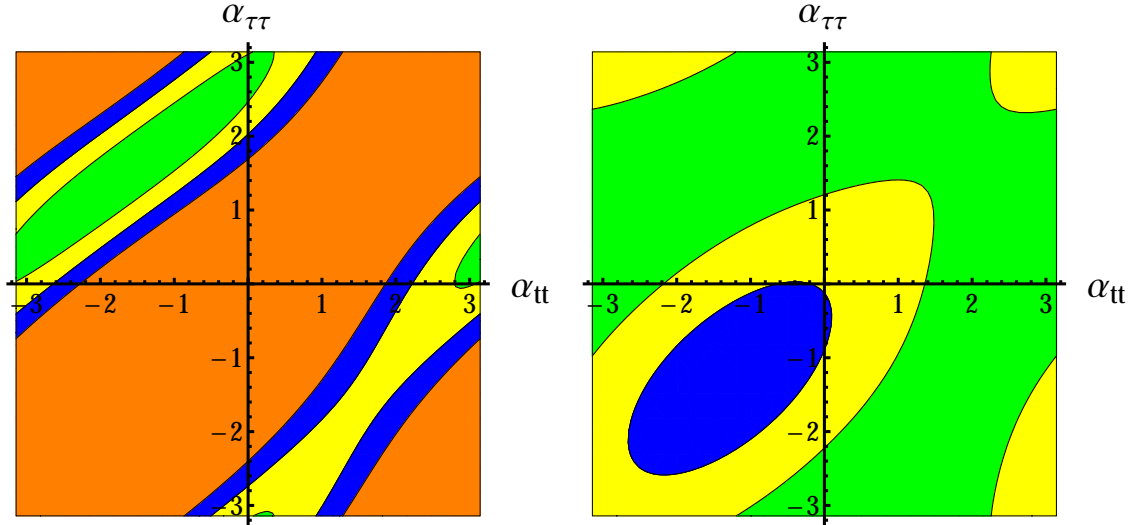
Another important indirect constraint on ξ_{tt} comes from the leptonic decay of B meson. Future measurements on $\text{Br}(B_s^0 \rightarrow \mu^+ \mu^-)$ would reach 12% with 3ab^{-1} luminosity by CMS [143] and 4% with 50fb^{-1} by LHCb [142]. If no deviation from SM were found, it would

require $|\xi_{tt}| \lesssim 0.4$ at 95% C.L. If $|\xi_{tt}| = 0.6$, the LHCb result would be larger than the SM prediction at 3σ level.

At LHC with $\sqrt{s} = 13\text{TeV}$ and 300fb^{-1} luminosity, if no LFV signal were found, it would require $\text{Br}(h \rightarrow \mu^\pm \tau^\mp) < 7.7 \times 10^{-4}$ at 95% C.L. [144], or equivalently $|\xi_{\mu\tau}| \lesssim (1.1 - 3.5)$ which is still not strict. To 3ab^{-1} , the upper limit for $|\xi_{\mu\tau}|$ would reduce to $(0.6 - 2.0)$. At SuperB factory with 75ab^{-1} luminosity, $\text{Br}(\tau \rightarrow \mu\gamma)$ can be constrained to less than 2.4×10^{-9} at 90% C.L., or be discovered at 3σ level if it is larger than 5.4×10^{-9} [140].

According to (76) and (78) taking the benchmark points in Table I, fix $|\xi_{\mu\tau}| = |\xi_{\tau\mu}| = |\xi_{\tau\tau}| = 1$ and $\xi_{tt} = 0.6$, we plot the $\text{Br}(\tau \rightarrow \mu\gamma)$ distributions in $\alpha_{tt} - \alpha_{\tau\tau}$ plane in Figure 17, for $m_\eta = 20\text{GeV}$ (left) and $m_\eta = 40\text{GeV}$ (right). If no evidence for $\tau \rightarrow \mu\gamma$ were found,

FIG. 17: Distributions of $\text{Br}(\tau \rightarrow \mu\gamma)$ in $\alpha_{tt} - \alpha_{\tau\tau}$ plane with the benchmark points in section III F. The left figure is for $m_\eta = 20\text{GeV}$ and the right figure is for $m_\eta = 40\text{GeV}$. In both figures, $|\xi_{\mu\tau}| = |\xi_{\tau\mu}| = |\xi_{\tau\tau}| = 1$ and $\xi_{tt} = 0.6$. The green regions are for $\text{Br}(\tau \rightarrow \mu\gamma) \leq 2.4 \times 10^{-9}$; the yellow regions are for $2.4 \times 10^{-9} < \text{Br}(\tau \rightarrow \mu\gamma) \leq 5.4 \times 10^{-9}$; the blue regions are for $5.4 \times 10^{-9} < \text{Br}(\tau \rightarrow \mu\gamma) \leq 9 \times 10^{-9}$; and the orange regions are for $\text{Br}(\tau \rightarrow \mu\gamma) > 9 \times 10^{-9}$.



the parameters would be constrained to be in green regions. While if the parameters were in blue (orange) regions, $\tau \rightarrow \mu\gamma$ would be discovered at $3(5)\sigma$ level at SuperB factory with 75ab^{-1} luminosity. Fixing $|\xi_{\mu\tau}| = |\xi_{\tau\mu}| = 1$ and leaving other parameters free, if no evidence were found at SuperB, $|\xi_{\tau\tau}|$ would be required less than 1.2 for the $m_\eta = 20\text{GeV}$ case or less than 2.6 for the $m_\eta = 40\text{GeV}$ case.

At SuperB factory, the dominant background for $\tau \rightarrow \mu\gamma$ should be $e^+e^- \rightarrow \tau^+\tau^-\gamma$ [139]

which would be suppressed at a collider with \sqrt{s} not far above $2m_\tau$, such as Super tau-charm factory [145]. At Super tau-charm factory with 10ab^{-1} luminosity, the sensitivity of $\text{Br}(\tau \rightarrow \mu\gamma)$ would reach around 2×10^{-10} [146], which can give further constraints. Future MEG experiments on $\text{Br}(\mu \rightarrow e\gamma)$ would reach the sensitivity 6×10^{-14} in three years [147], which can give stricter constraints for all the three LFV couplings $\xi_{e\mu, e\tau, \mu\tau}$.

V. CONCLUSIONS AND DISCUSSIONS

In this paper, based on weakly-coupled spontaneous CP-violation 2HDM (named Lee model), using the correlation between the lightest scalar and smallness of CP-violation through small $t_\beta s_\xi$ which was proposed in our recent paper [1], we predicted that a light CP-mixing scalar with its mass of $\mathcal{O}(10\text{GeV})$ should exist. It is pseudoscalar dominant with only about $\mathcal{O}(0.1)$ scalar component. In this scenario, other scalars' masses are all around the electro-weak scale v . It's attractive because there should be new physics hidden at $\mathcal{O}(10\text{GeV})$ scale which is below the electro-weak scale, different from the scenario we discussed in [1] in which the Higgs sector is strong-coupled and new physics appear at $\mathcal{O}(\text{TeV})$ or higher scale.

We discussed all experimental constraints, at both high and low energy, for two typical lightest scalar (η) masses, $m_\eta = 20\text{GeV}$ ($h \rightarrow Z\eta$ decay allowed) and $m_\eta = 40\text{GeV}$ ($h \rightarrow Z\eta$ decay forbidden). For these η masses, $c_{\eta,V} \sim 0.1$ is required theoretically and it is also allowed by data. The 125 GeV Higgs boson h has SM-like couplings to fermions and gauge bosons. With a global-fit to higgs signal strengths, branching ratio for exotic decay channels are constrained to less than about 30%, which leads to strict constraints on $h\eta\eta$ (and $hZ\eta$ if $m_\eta < 34\text{GeV}$) couplings. The constraints from oblique parameters require $m_\pm \sim m_H \sim v$ under the weak-coupling assumption. The typical benchmark points listed in Table I are chosen according to these constraints.

In Lee model, there is no additional discrete symmetry except CP, thus there may exist flavor-changing interactions at tree level. We adopted the Cheng-Sher ansatz to parameterize the flavor-changing effects. High energy processes including top flavor-changing interactions cannot give strict constraints. The most strict constraint from high energy experiments comes from an indirect test, top quark widths limit from $t\bar{t}$ pair production, which requires $|\xi_{tc}| \lesssim 1$. A more strict constraint comes from $D^0 - \bar{D}^0$ mixing which requires $|\xi_{tc}\xi_{tu}| \lesssim 6$. All

other $|\xi_{ij}|$ in quark sector are constrained to be less than around $\mathcal{O}(10^{-2})$, through meson mixing measurements. In lepton sector, indirect tests (especially radiative LFV decays) require $|\xi_{\mu\tau}| \lesssim \mathcal{O}(1)$, while upper limit on $|\xi_{e\mu}|$ or $|\xi_{e\tau}\xi_{\mu\tau}|$ are of $\mathcal{O}(10^{-2})$. EDM tests also favor $|\xi_{e\tau,ut}| \lesssim \mathcal{O}(1)$. These constraints are usually stricter than those in [1] as we discussed, that's because in this scenario, a lighter scalar would give more significant contribution to the flavor-changing processes.

B meson mixing and B leptonic decay processes are all sensitive to ξ_{tt} . With these data, $|\xi_{tt}| \lesssim 0.6$ is favored at 95% C.L. which is the reason why in most part of the text we choose $|\xi_{tt}| = 0.6$ as a benchmark point. The B radiative decay process is sensitive to both ξ_{tt} and ξ_{bb} . With the assumption $m_{\pm} \sim (200 - 300)\text{GeV}$ and $|\xi_{tt}| = 0.6$, $\xi_{bb} \lesssim \mathcal{O}(1)$ is allowed by data. That is a difference between this scenario and type II 2HDM in which charged Higgs should be heavier than around 410 GeV at 95% C.L.

The EDM constraints are also strict just like the scenario we discussed in [1]. For both electron and neutron EDM, we need large cancelation between different contributions, as shown in Figure 8-Figure 14. In each of the figures, the two shown parameters are constrained in a narrow band which means a strong correlation between them.

We also discussed the future tests for this scenario. For the lightest scalar η , the dominant ways to discover it at LHC are associated production $pp \rightarrow t\bar{t}\eta$ and cascade decay $pp \rightarrow h, H \rightarrow \eta\eta, Z\eta$. While since the heaviest neutral scalar is also required to have its mass around v , it can also be searched through $Z\eta$ or VV final states. At LHeC or e^+e^- colliders, the exotic decays $h \rightarrow \eta\eta, Z\eta$ would be tested. Especially at Higgs factory, with $\mathcal{O}(10 - 10^2)\text{fb}^{-1}$ luminosity, $c_{\eta,V} \sim 0.1$ can be discovered at $(3 - 5)\sigma$ through re-scaling the LEP constraints. If nothing were found, constraints on $c_{\eta,V}$ would improve an order which also implies $m_{\eta} \sim \mathcal{O}(\text{GeV})$, thus this scenario is disfavored. The mass of charged Higgs boson is predicted to be around v which is possible to be discovered at future LHC or e^+e^- colliders with $\sqrt{s} \gtrsim 500\text{GeV}$, using $\mathcal{O}(0.1 - 1)\text{ab}^{-1}$ luminosity. Note that the $e^+e^- \rightarrow H^+H^-$ process cannot be suppressed with fixed m_{\pm} , if nothing were found, this scenario would be excluded.

If all the three scalars are discovered and they all have direct vertices to massive gauge boson pairs, the Z -mediated Higgs associated pair production via $e^+e^- \rightarrow h_i h_j$ would be a key observable to confirm CP-violation in scalar sector. It can be used to distinguish Lee model and models in which the scalar sector contains more CP-even degrees of freedom but no CP-violation.

Indirect tests on B meson mixing and B leptonic decay can be used to test a nonzero ξ_{tt} or give a stricter limit on $|\xi_{tt}|$. For the case $|\xi_{tt}| = 0.6$ we used in this paper, there would appear $(3 - 5)\sigma$ deviations in these experiments. If nothing anomaly were found, $|\xi_{tt}|$ would be pushed to less than about $(0.2 - 0.3)$. Radiative LFV decays would also confirm a nonzero LFV vertex or push them to a smaller number, depending on the results positive or negative.

In this attractive scenario, all new physics would appear below or at electro-weak scale which behaves different from most models in which new physics appear at or above $\mathcal{O}(\text{TeV})$ scale. It means this scenario is testable. The roughly estimation showed it is able to discover or exclude this scenario, especially for η who is hidden at $\mathcal{O}(10\text{GeV})$ scale. It is also possible to distinguish whether CP-violation in Higgs sector exists if all neutral scalars were found. Thus it is worth further studying in details, especially at future e^+e^- colliders.

Acknowledgement

We thank Chen Zhang for helpful discussions. This work was supported in part by the Natural Science Foundation of China (Grants No. 11135003 and No. 11375014).

Appendix A: Spectrum and Couplings

Expansion for the neutral scalar mass matrix

$$\begin{pmatrix} (\lambda_4 - \lambda_7)s_\xi^2 & -((\lambda_4 - \lambda_7)s_\beta c_\xi + \lambda_2 c_\beta)s_\xi & -((\lambda_4 - \lambda_7)c_\beta c_\xi + \lambda_5 s_\beta)s_\xi \\ & 4\lambda_1 c_\beta^2 + \lambda_2 s_{2\beta} c_\xi + (\lambda_4 - \lambda_7)s_\beta^2 c_\xi^2 & ((\lambda_3 + \lambda_7) + (\lambda_4 - \lambda_7)c_\xi^2/2)s_{2\beta} \\ & & + \lambda_2 c_\beta^2 c_\xi + \lambda_5 s_\beta^2 c_\xi \\ & & (\lambda_4 - \lambda_7)c_\beta^2 c_\xi^2 \\ & & + \lambda_5 s_{2\beta} c_\xi + 4\lambda_6 s_\beta^2 \end{pmatrix} \quad (\text{A.1})$$

is $\tilde{m} = \tilde{m}_0 + (t_\beta s_\xi)\tilde{m}_1 + (t_\beta s_\xi)^2\tilde{m}_2 + \dots$. To the first order, we have

$$m_\eta = 0, \quad m_{h,H} = \frac{v}{2}\sqrt{(4\lambda_1 + \lambda_4 - \lambda_7) \mp ((4\lambda_1 - (\lambda_4 - \lambda_7))c_{2\theta} + 2\lambda_2 s_{2\theta})} \quad (\text{A.2})$$

where $\theta = (1/2) \arctan(2\lambda_2/(4\lambda_1 - \lambda_4 + \lambda_7))$ is the mixing angle. The scalar fields

$$\eta_0 = I_2, \quad \begin{pmatrix} h \\ H \end{pmatrix}_0 = \begin{pmatrix} c_\theta & s_\theta \\ -s_\theta & c_\theta \end{pmatrix} \begin{pmatrix} R_1 \\ R_2 \end{pmatrix}. \quad (\text{A.3})$$

Calculation by perturbation method to the leading order of $(t_\beta s_\xi)$ gives

$$\eta = I_2 - (t_\beta s_\xi) \left(\frac{(\tilde{m}_1)_{12}}{(\tilde{m}_0)_{22}} (c_\theta R_1 + s_\theta R_2) + \frac{(\tilde{m}_1)_{13}}{(\tilde{m}_0)_{33}} (c_\theta R_2 - s_\theta R_1) \right) - t_\beta c_\xi I_1; \quad (\text{A.4})$$

$$h = c_{\theta'} R_1 + s_{\theta'} R_2 + \frac{(\tilde{m}_1)_{12}}{(\tilde{m}_0)_{22}} (t_\beta s_\xi) I_2; \quad (\text{A.5})$$

$$H = -s_{\theta'} R_1 + c_{\theta'} R_2 + (t_\beta s_\xi) \left(I_1 + \frac{(\tilde{m}_1)_{13}}{(\tilde{m}_0)_{33}} I_2 \right); \quad (\text{A.6})$$

$$m_\eta = \frac{v t_\beta s_\xi}{\sqrt{2}} \sqrt{(\tilde{m}_2)_{11} - \frac{(\tilde{m}_1)_{12}^2}{(\tilde{m}_0)_{22}} - \frac{(\tilde{m}_1)_{13}^2}{(\tilde{m}_0)_{33}}}. \quad (\text{A.7})$$

Here

$$\theta' = \theta + \frac{(t_\beta s_\xi)(\tilde{m}_1)_{23}}{(\tilde{m}_0)_{22} - (\tilde{m}_0)_{33}}. \quad (\text{A.8})$$

The scalar self-interactions

$$\mathcal{L} = - \sum \left(\frac{1}{S_{ijk}} g_{ijk} v h_i h_j h_k + \frac{1}{S_{ijkl}} g_{ijkl} h_i h_j h_k h_l \right) \quad (\text{A.9})$$

where the symmetric factor $S \equiv \prod(n_i!)$ in which n_i denotes the appearance time for h_i in the lagrangian. The couplings can be obtained directly from

$$g_{ijk} = \frac{1}{v} \frac{\partial^3 V}{\partial h_i \partial h_j \partial h_k} \Big|_{\text{all } h_i=0}, \quad g_{ijkl} = \frac{\partial^4 V}{\partial h_i \partial h_j \partial h_k \partial h_l} \Big|_{\text{all } h_i=0}. \quad (\text{A.10})$$

As an example, the $h\eta\eta$ vertex is given by

$$\begin{aligned} g_{h\eta\eta} &= \frac{\partial^3 V}{\partial h \partial \eta^2} \\ &= (\lambda_3 + \lambda_7) c_{\theta'} + \frac{1}{2} \lambda_5 s_{\theta'} - \frac{t_\beta c_\xi}{2} (\lambda_2 c_{\theta'} + (\lambda_4 - \lambda_7) s_{\theta'}). \end{aligned} \quad (\text{A.11})$$

For $m_\eta < m_h/2$, The strict constraints from $h \rightarrow \eta\eta$ rare decay showed that

$$\lambda_3 + \lambda_7 + \frac{\lambda_5 t_{\theta'}}{2} \simeq \frac{t_\beta c_\xi}{2} (\lambda_2 + (\lambda_4 - \lambda_7) t_{\theta'}) \quad (\text{A.12})$$

which means $(\tilde{m}_1)_{12} \sim \mathcal{O}(\beta)$ is ignorable in the formula above.

For the $h_i V V$ and $h_i h_j Z$ couplings, the effective interaction should be written as

$$\mathcal{L}_{h_i V V} = c_{i,V} h_i \left(\frac{2m_W^2}{v} W^{+\mu} W_\mu^- + \frac{m_Z^2}{v} Z^\mu Z_\mu \right); \quad (\text{A.13})$$

$$\mathcal{L}_{h_i h_j Z} = \frac{c_{ij} g}{2c_W} Z^\mu (h_i \partial_\mu h_j - h_j \partial_\mu h_i). \quad (\text{A.14})$$

With a straightforward calculation, we have

$$c_{\eta,V} = c_{hH}, \quad c_{h,V} = c_{H\eta}, \quad c_{H,V} = c_{\eta h} \quad (\text{A.15})$$

thus $\sum c_{i,V}^2 = \sum c_{ij}^2 = 1$. In this scenario, to the leading order of $t_\beta s_\xi$,

$$c_{\eta,V} = t_\beta s_\xi \left(1 + s_\theta \frac{(\tilde{m}_1)_{13}}{(\tilde{m}_0)_{33}} - c_\theta \frac{(\tilde{m}_1)_{12}}{(\tilde{m}_0)_{22}} \right); \quad (\text{A.16})$$

$$c_{h,V} = c_{\theta'} + t_\beta c_\xi s_{\theta'}; \quad (\text{A.17})$$

$$c_{H,V} = -s_{\theta'} + t_\beta c_\xi c_{\theta'}. \quad (\text{A.18})$$

For the case $m_\eta < m_h - m_Z$, strict constraints from $h \rightarrow Z\eta$ rare decay showed that $c_{H,V} \ll 1$ thus $t_{\theta'} \simeq t_\beta c_\xi$.

The Yukawa interactions

$$\mathcal{L}_Y = - \sum_\phi \left(\sum_f \frac{c_{\phi,f} m_f}{v} \bar{f}_L f_R \phi + \sum_{i \neq j} \frac{c_{\phi,ij} \sqrt{m_i m_j}}{v} \bar{f}_{Li} f_{Rj} \phi \right) + \text{h.c.} \quad (\text{A.19})$$

where ϕ denotes any scalar and f denotes any fermion. The factors for diagonal terms can be generated directly as

$$c_{\eta,f} = \pm i \xi_{ff} \left(1 + t_\beta s_\xi \left(\frac{(\tilde{m}_1)_{12}}{(\tilde{m}_0)_{22}} c_{\theta'} - \frac{(\tilde{m}_1)_{13}}{(\tilde{m}_0)_{33}} s_{\theta'} \right) \right) + t_\beta s_\xi \left(1 - c_{\theta'} \left(\xi_{ff} \frac{(\tilde{m}_1)_{12}}{(\tilde{m}_0)_{22}} + \frac{(\tilde{m}_1)_{13}}{(\tilde{m}_0)_{33}} \right) - s_{\theta'} \left(\xi_{ff} \frac{(\tilde{m}_1)_{12}}{(\tilde{m}_0)_{22}} - \frac{(\tilde{m}_1)_{13}}{(\tilde{m}_0)_{33}} \right) \right); \quad (\text{A.20})$$

$$c_{h,f} = c_{\theta'} + \xi_{ff} s_{\theta'} + t_\beta c_\xi (s_{\theta'} - \xi_{ff} c_{\theta'}) \pm i t_\beta s_\xi \xi_{ff} \left(\frac{(\tilde{m}_1)_{12}}{(\tilde{m}_0)_{22}} - c_{\theta'} \right); \quad (\text{A.21})$$

$$c_{H,f} = -s_{\theta'} + \xi_{ff} c_{\theta'} + t_\beta c_\xi (c_{\theta'} + \xi_{ff} s_{\theta'}) \pm i t_\beta s_\xi \xi_{ff} \left(\frac{(\tilde{m}_1)_{13}}{(\tilde{m}_0)_{33}} + s_{\theta'} \right). \quad (\text{A.22})$$

While the factors for off-diagonal term are

$$c_{\eta,ij} = \pm i \xi_{ij} \left(1 + t_\beta s_\xi \left(\frac{(\tilde{m}_1)_{12}}{(\tilde{m}_0)_{22}} c_{\theta'} - \frac{(\tilde{m}_1)_{13}}{(\tilde{m}_0)_{33}} s_{\theta'} \right) \right) - t_\beta s_\xi \xi_{ij} \left(c_{\theta'} \frac{(\tilde{m}_1)_{13}}{(\tilde{m}_0)_{33}} + s_{\theta'} \frac{(\tilde{m}_1)_{12}}{(\tilde{m}_0)_{22}} \right); \quad (\text{A.23})$$

$$c_{h,ij} = \xi_{ij} \left(s_{\theta'} - t_\beta c_\xi c_{\theta'} \pm i t_\beta s_\xi \left(\frac{(\tilde{m}_1)_{12}}{(\tilde{m}_0)_{22}} - c_{\theta'} \right) \right); \quad (\text{A.24})$$

$$c_{H,ij} = \xi_{ij} \left(c_{\theta'} + t_\beta c_\xi s_{\theta'} \pm i t_\beta s_\xi \left(\frac{(\tilde{m}_1)_{13}}{(\tilde{m}_0)_{33}} + s_{\theta'} \right) \right). \quad (\text{A.25})$$

In each of the six formula, when “ \pm ” appears, “ $+$ ” stands for down type fermions and “ $-$ ” stands for up type fermions.

Appendix B: Useful Analytical Loop Integrations

The loop integration functions for $h \rightarrow \gamma\gamma(gg)$ decay width in (40) and (41) are

$$\mathcal{A}_0(x) = \frac{x - f(x)}{x^2}, \quad (\text{B.1})$$

$$\mathcal{A}_{1/2}(x) = -\frac{x + (x-1)f(x)}{x^2}, \quad (\text{B.2})$$

$$\mathcal{B}_{1/2}(x) = -\frac{2f(x)}{x}, \quad (\text{B.3})$$

$$\mathcal{A}_1(x) = \frac{2x^2 + 3x + 3(2x-1)f(x)}{x^2} \quad (\text{B.4})$$

where

$$f(x) = \begin{cases} \arcsin^2(\sqrt{x}), & (\text{for } x \leq 1); \\ -\frac{1}{4} \left(\ln \frac{1+\sqrt{1-x^{-1}}}{1-\sqrt{1-x^{-1}}} - i\pi \right), & (\text{for } x > 1). \end{cases} \quad (\text{B.5})$$

The difference between $\mathcal{A}_{1/2}$ and $\mathcal{B}_{1/2}$ comes from the different tensor structures for the scalar and pseudoscalar components.

The loop integration functions for oblique parameters in (50) and (51) are

$$F(x, y) = \frac{x+y}{2} - \frac{xy}{x-y} \ln \left(\frac{x}{y} \right); \quad (\text{B.6})$$

$$G(x, y) = -\frac{16}{3} + 5(x+y) - 2(x-y)^2 + 3 \left(\frac{x^2+y^2}{x-y} + y^2 - x^2 + \frac{(x-y)^3}{3} \right) \ln \left(\frac{x}{y} \right) \\ + (1 - 2(x+y) + (x-y)^2) f(x+y-1, 1 - 2(x+y) + (x-y)^2); \quad (\text{B.7})$$

$$H(x) = -\frac{79}{3} + 9x - 2x^2 + \left(-10 + 18x - 6x^2 + x^3 - 9\frac{x+1}{x-1} \right) \ln x \\ + (12 - 4x + x^2) f(x, x^2 - 4x); \quad (\text{B.8})$$

where

$$f(x, y) = \begin{cases} \sqrt{y} \ln \left| \frac{x-\sqrt{y}}{x+\sqrt{y}} \right|, & y \geq 0; \\ 2\sqrt{-y} \arctan \left(\frac{\sqrt{-y}}{x} \right), & y < 0. \end{cases} \quad (\text{B.9})$$

The loop integration functions for meson mixing in (55) and (57) are

$$\mathcal{F}_0(x) = \frac{x(1-x^2+2x \ln x)}{(1-x)^3}; \quad (\text{B.10})$$

$$\mathcal{F}_1(x, y, z) = \frac{2y}{1-z} \left(\frac{(z-4) \ln y}{(1-y)^2} + \frac{3z \ln x}{(1-x)^2} - \frac{(1-z)(4-x)}{(1-y)(1-x)} \right); \quad (\text{B.11})$$

$$\mathcal{F}_2(x) = 1 + \frac{9}{1-x} - \frac{6}{(1-x)^2} - \frac{6x^2 \ln x}{(1-x)^3}. \quad (\text{B.12})$$

The loop integration functions for two-loop radiative LFV τ decay in (74) are

$$f(z) = \frac{z}{2} \int_0^1 dx \frac{1-2x(1-x)}{x(1-x)-z} \ln \left(\frac{x(1-x)}{z} \right); \quad (\text{B.13})$$

$$g(z) = \frac{z}{2} \int_0^1 dx \frac{1}{x(1-x)-z} \ln \left(\frac{x(1-x)}{z} \right); \quad (\text{B.14})$$

$$h(z) = -\frac{z}{2} \int_0^1 dx \frac{1}{x(1-x)-z} \left(1 - \frac{z}{x(1-x)-z} \ln \left(\frac{x(1-x)}{z} \right) \right). \quad (\text{B.15})$$

For $z < 1/4$, the integrations are defined as their Cauchy principle value.

The loop integration functions for two-loop Barr-Zee type contribution in calculating the EDM for a fermion f in (87) are

$$\mathcal{J}_0(m_{\pm}, m_{\phi}) = \frac{v^2}{2m_{\phi}^2} \left(\mathcal{I} \left(\frac{m_{\pm}^2}{m_{\phi}^2} \right) - \mathcal{I}' \left(\frac{m_{\pm}^2}{m_{\phi}^2} \right) \right); \quad (\text{B.16})$$

$$\mathcal{J}_{1/2}(m_t, m_{\phi}) = \frac{m_t^2}{m_{\phi}^2} \mathcal{I} \left(\frac{m_t^2}{m_{\phi}^2} \right); \quad (\text{B.17})$$

$$\mathcal{J}'_{1/2}(m_t, m_{\phi}) = \frac{m_t^2}{m_{\phi}^2} \mathcal{I}' \left(\frac{m_t^2}{m_{\phi}^2} \right); \quad (\text{B.18})$$

$$\mathcal{J}_1(m_W, m_{\phi}) = \frac{m_W^2}{m_{\phi}^2} \left(\left(5 - \frac{m_{\phi}^2}{2m_W^2} \right) \mathcal{I} \left(\frac{m_W^2}{m_{\phi}^2} \right) + \left(3 + \frac{m_{\phi}^2}{2m_W^2} \right) \mathcal{I}' \left(\frac{m_W^2}{m_{\phi}^2} \right) \right); \quad (\text{B.19})$$

where

$$\mathcal{I}(z) = \int_0^1 dx \frac{1}{x(1-x)-z} \ln \left(\frac{x(1-x)}{z} \right); \quad (\text{B.20})$$

$$\mathcal{I}'(z) = \int_0^1 dx \frac{1-2x(1-x)}{x(1-x)-z} \ln \left(\frac{x(1-x)}{z} \right). \quad (\text{B.21})$$

For $z < 1/4$, the integrations are defined as their Cauchy principle value as above. The loop function for Weinberg operator in (91) is

$$\mathcal{K}(x) = 4x^2 \int_0^1 du \int_0^1 dv \frac{(uv)^3(1-v)}{(xv(1-uv) + (1-u)(1-v))^2}. \quad (\text{B.22})$$

The loop functions for one-loop contribution to fermion EDM in (93)-(94) and (98) are

$$\mathcal{P}_1(x) = \frac{x}{(x-1)^2} \left(\frac{x-3}{2} + \frac{\ln x}{x-1} \right); \quad (\text{B.23})$$

$$\mathcal{P}_2(x) = \int_0^1 dz \frac{z^2}{1-z+xz^2}. \quad (\text{B.24})$$

The loop integration functions for B meson leptonic decays in (95) are

$$\mathcal{Y}_{\text{SM}}(x) = \frac{x}{8} \left(\frac{x-4}{x-1} + \frac{3x \ln x}{(x-1)^2} \right); \quad (\text{B.25})$$

$$\mathcal{Y}_{2\text{HDM}}(x) = \frac{x^2}{8} \left(\frac{1}{y-x} + \frac{y}{(y-x)^2} \ln \left(\frac{x}{y} \right) \right). \quad (\text{B.26})$$

Appendix C: Formalism for Meson Mixing

Begin with the Schrödinger equation

$$i \frac{\partial}{\partial t} |\psi\rangle = \mathcal{H} |\psi\rangle = \left(\mathbf{m} - \frac{i}{2} \mathbf{\Gamma} \right) |\psi\rangle \quad (\text{C.1})$$

where $|\psi\rangle = (|M^0\rangle, |\bar{M}^0\rangle)^T$ with normalization condition $\langle M^0 | M^0 \rangle = \langle \bar{M}^0 | \bar{M}^0 \rangle = 2m_M$ in position space, and $\mathbf{m}, \mathbf{\Gamma}$ are 2×2 matrixes. The hamiltonian can be written as

$$\mathcal{H} = \mathcal{H}_0 + \mathcal{H}_{\Delta F=1} + \mathcal{H}_{\Delta F=2}. \quad (\text{C.2})$$

The matrix element

$$\left(\mathbf{m} - \frac{i}{2} \mathbf{\Gamma} \right)_{ij} = m_M \delta_{ij} + \frac{1}{2m_M} \langle \psi_i | \mathcal{H}_{\Delta F=2} | \psi_j \rangle + \frac{1}{2m_M} \int d\Pi_f \frac{\langle \psi_i | \mathcal{H}_{\Delta F=1} | f \rangle \langle f | \mathcal{H}_{\Delta F=1} | \psi_j \rangle}{m_M - E_f + i\epsilon} \quad (\text{C.3})$$

where the states $|\psi_{i,j}\rangle$ mean $|M^0\rangle$ or $|\bar{M}^0\rangle$, and $|f\rangle$ denotes a mediated state. The second and third terms correspond to short- and long-distance contributions respectively, and from the third term,

$$\mathbf{\Gamma}_{ij} = \frac{1}{2m_M} \int d\Pi_f \langle \psi_i | \mathcal{H}_{\Delta F=1} | f \rangle \langle f | \mathcal{H}_{\Delta F=1} | \psi_j \rangle 2\pi \delta(E_f - m_M). \quad (\text{C.4})$$

The masses and widths for the mass eigenstates are

$$m_{H(L)} = m_M \pm \text{Re} \left(\sqrt{\left(\mathbf{m}_{12} - \frac{i}{2} \mathbf{\Gamma}_{12} \right) \left(\mathbf{m}_{12}^* - \frac{i}{2} \mathbf{\Gamma}_{12}^* \right)} \right); \quad (\text{C.5})$$

$$\Gamma_{H(L)} = \Gamma_M \mp \text{Im} \left(\sqrt{\left(\mathbf{m}_{12} - \frac{i}{2} \mathbf{\Gamma}_{12} \right) \left(\mathbf{m}_{12}^* - \frac{i}{2} \mathbf{\Gamma}_{12}^* \right)} \right); \quad (\text{C.6})$$

where H (L) denotes the heavy (light) mass eigenstate

$$|M_{H(L)}\rangle = p|M^0\rangle \mp q|\bar{M}^0\rangle. \quad (\text{C.7})$$

p and q are determined through

$$|p|^2 + |q|^2 = 1, \quad \text{and} \quad \left(\frac{p}{q}\right)^2 = \frac{\mathbf{m}_{12} - i\mathbf{\Gamma}_{12}/2}{\mathbf{m}_{12}^* - i\mathbf{\Gamma}_{12}^*/2}. \quad (\text{C.8})$$

In $K^0 - \bar{K}^0$ system, \mathbf{m}_{12} is almost real and $\mathbf{\Gamma}_{12} \sim \mathbf{m}_{12}$, thus $\Delta m_K \approx 2\text{Re}\mathbf{m}_{12}$; while in $B_{(s)}^0 - \bar{B}_{(s)}^0$ system, $|\mathbf{\Gamma}_{12}| \ll |\mathbf{m}_{12}|$, thus $\Delta m_B \approx 2|\mathbf{m}_{12}|$.

Transform to momentum space, take \mathcal{H} as the hamiltonian density and change the normalization condition to $\langle M^0 | M^0 \rangle = \langle \bar{M}^0 | \bar{M}^0 \rangle = 2m_M \delta^{(3)}(\mathbf{p})$. With the matrix elements

$$\langle 0 | \bar{f}_i \gamma^\mu \gamma^5 f_j | M^0(p) \rangle = -i f_M p^\mu, \quad \langle 0 | \bar{f}_i \gamma^5 f_j | M^0(p) \rangle = i \frac{m_M^2 f_M}{m_i + m_j}; \quad (\text{C.9})$$

the useful $\Delta F = 2$ matrix elements

$$\langle \bar{M}_0 | \bar{f}_{Li} \gamma^\mu f_{Lj} \bar{f}_{Li} \gamma_\mu f_{Lj} | M_0 \rangle = \langle \bar{M}_0 | \bar{f}_{Ri} \gamma^\mu f_{Rj} \bar{f}_{Ri} \gamma_\mu f_{Rj} | M_0 \rangle = \frac{2}{3} f_M^2 m_M^2; \quad (\text{C.10})$$

$$\langle \bar{M}_0 | \bar{f}_{Li} \gamma^\mu f_{Lj} \bar{f}_{Ri} \gamma_\mu f_{Rj} | M_0 \rangle = -\frac{5}{6} f_M^2 m_M^2; \quad (\text{C.11})$$

$$\langle \bar{M}_0 | \bar{f}_{Li} f_{Rj} \bar{f}_{Li} f_{Rj} | M_0 \rangle = \langle \bar{M}_0 | \bar{f}_{Ri} f_{Lj} \bar{f}_{Ri} f_{Lj} | M_0 \rangle = -\frac{5}{12} f_M^2 m_M^2; \quad (\text{C.12})$$

$$\langle \bar{M}_0 | \bar{f}_{Li} f_{Rj} \bar{f}_{Ri} f_{Lj} | M_0 \rangle = \frac{7}{12} f_M^2 m_M^2; \quad (\text{C.13})$$

where the bag parameters are all taken as 1 for simplify.

-
- [1] Y.-N. Mao and S.-H. Zhu, Phys. Rev. D 90, 115024 (2014).
 - [2] F. Englert and R. Brout, Phys. Rev. Lett. 13, 321 (1964); P. W. Higgs, Phys. Rev. Lett. 13, 508 (1964); G. S. Guralnik, C. R. Hagen, and T. W. B. Kibble, Phys. Rev. Lett. 13, 585 (1964).
 - [3] G. C. Branco, P. M. Ferreira, L. Lavoura, M. N. Rebelo, M. Sher, and J. P. Silva, Phys. Rep. 516, 1 (2012).
 - [4] The ATLAS Collaboration, Phys. Lett. B 716, 1 (2012).
 - [5] The CMS Collaboration, Phys. Lett. B 716, 30 (2012).
 - [6] The ATLAS and CMS Collaborations, Phys. Rev. Lett. 114, 191803 (2015).
 - [7] The ATLAS Collaboration, Report No. ATLAS-CONF-2015-007.
 - [8] M. Flechl (the ATLAS and CMS Collaborations), arXiv:1503.00632.
 - [9] The ATLAS and CMS Collaborations, Report No ATLAS-CONF-2015-044.

- [10] J. Ellis, J. F. Gunion, H. E. Haber, L. Roszkowski, and F. Zwirner, Phys. Rev. D 39, 844 (1989).
- [11] D. E. Kaplan and M. Schmaltz, JHEP 0310, 039 (2003).
- [12] K. Cheung and J. Song, Phys. Rev. D 76, 035007 (2007).
- [13] K. Cheung, J. Song, P. Tseng, and Q.-S. Yan, Phys. Rev. D 78, 055015 (2008).
- [14] Z. Chacko, H.-S. Goh, and R. Harnik, Phys. Rev. Lett. 96, 231802 (2006); JHEP 0601, 108 (2006).
- [15] Y.-B. Liu and Z.-J. Xiao, JHEP 02, 128 (2014).
- [16] J.-M. Gérard and M. Herquet, Phys. Rev. Lett. 98, 251802 (2007).
- [17] B. Coleppa, F. Kling, and S. Su, JHEP 1401, 161 (2014), arXiv:1305.0002; arXiv: 1308.6201.
- [18] L. Wang and X.-F. Han, JHEP 1505, 039 (2015).
- [19] B. Dumont, J. F. Gunion, Y. Jiang, and S. Kraml, Phys. Rev. D 90, 035021 (2014).
- [20] J. Bernon, J. F. Gunion, Y. Jiang, and S. Kraml, Phys. Rev. D 91, 075019 (2015).
- [21] D. Curtin et. al., Phys. Rev. D 90, 075004 (2014).
- [22] S. Chatrchyan et. al. (the CMS Collaboration), Phys. Rev. D 89, 092007 (2014).
- [23] The CMS Collaboration, Report No. CMS-PAS-HIG-14-014.
- [24] The ATLAS Collaboration, Report No. ATLAS-CONF-2015-008.
- [25] M. Kobayashi and T. Maskawa, Prog. Theor. Phys. 49, 652 (1973).
- [26] N. Cabibbo, Phys. Rev. Lett. 10, 531 (1963).
- [27] L. Wolfenstein, Phys. Rev. Lett. 51, 1945 (1983).
- [28] C. Jarlskog, Phys. Rev. Lett. 55, 1039 (1985).
- [29] K. A. Olive et. al. (Particle Data Group), Chin. Phys. C 38, 090001 (2014).
- [30] The Planck Collaboration, Astron. Astrophys. 571, A16 (2014).
- [31] A. G. Cohen, D. B. Kaplan, and A. E. Nelson, Phys. Lett. B 263, 86 (1991); Annu. Rev. Nucl. Part. Sci. 43, 27 (1993).
- [32] D. E. Morrissey and M. J. Ramsey-Musolf, New J. Phys. 14, 125003 (2012).
- [33] J. Shu and Y. Zhang, Phys. Rev. Lett. 111, 091801 (2013).
- [34] T. D. Lee, Phys. Rev. D 8, 1226 (1973); Phys. Rep. 9, 143 (1974).
- [35] A. Méndez and A. Pomaral, Phys. Lett. B 272, 313 (1991).
- [36] S.-H. Zhu, arXiv: 1410.2042.
- [37] J. D. Bjorken and S. Weinberg, Phys. Rev. Lett. 38, 622 (1977).

- [38] S. L. Chen, N. G. Deshpande, X. G. He, J. Jiang, and L. H. Tsai, Eur. Phys. J. C 53, 607 (2008).
- [39] W. Liao, (2014) http://125.217.162.12/~zhanghonghao/tev2014/tev2014ppt/TeV2014_3a_Liaowei.pdf.
- [40] T. P. Cheng and M. Sher, Phys. Rev. D 35, 3484 (1987).
- [41] B. Pontecorvo, Zh. Eksp. Teor. Fiz. 33, 549 (1957) [Sov. Phys. JEPT 6, 429 (1957)]; Z. Maki, M. Nakagawa, and S. Sakata, Prog. Theor. Phys. 28, 870 (1962).
- [42] M. Ablikim et. al. (the BESIII Collaboration), Reports No. BAM-00180 and No. BAM-000402, arXiv: 1510.01641.
- [43] B. Aubert et. al. (BaBar Collaboration), Phys. Rev. Lett. 103, 081803 (2009).
- [44] V. Prasad, Reports No. SLAC-R-1008 and No. BABAR-THESIS-13-001 (PhD Thesis), arXiv: 1307.4560.
- [45] The CMS Collaboration, Phys. Rev. Lett. 109, 121801 (2012).
- [46] The CMS Collaboration, Report No. CMS-HIG-14-033, arXiv: 1511.03610.
- [47] The ACME Collaboration, Science 343, 269 (2014).
- [48] C. Baker et. al., Phys. Rev. Lett. 97, 131801 (2006).
- [49] M. Pospelov and A. Ritz, Ann. Phys. (Amsterdam) 318, 119 (2005).
- [50] G. Abbiendi et. al., (ALEPH, DELPHI, L3, and OPAL Collaborations, the LEP Higgs Working Group), Phys. Lett. B 565, 61 (2003).
- [51] The ALEPH, DELPHI, L3, and OPAL Collaborations (the LEP Higgs Working Group), Eur. Phys. J. C 47, 547 (2006).
- [52] The ALEPH, DELPHI, L3, and OPAL Collaborations (the LEP Higgs Working Group), Report No. LHWG Note/2001-04, arXiv: hep-ex/0107030.
- [53] P. Mario (the CMS Collaboration), Report No. CMS-CR-2015-045.
- [54] The ATLAS Collaboration, JHEP 1601, 032 (2016).
- [55] The LHC Higgs Cross Section Working Group, Report No. CERN-2013-004, arXiv: 1307.1347.
- [56] The CMS Collaboration, Phys. Lett. B 749, 560 (2015).
- [57] The ATLAS Collaboration, Report No. CERN-PH-EP-2015-290, arXiv: 1512.03704.
- [58] A. Djouadi, Phys. Rep. 457, 1 (2008).
- [59] A. Djouadi, Phys. Rep. 459, 1 (2008).

- [60] M. Baak, J. Cuth, J. Haller, A. Hoecker, R. Kogler, K. Mönig, M. Schott, and J. Stelzer, Eur. Phys. J. C 74, 3046 (2014).
- [61] M. E. Peskin and T. Takeuchi, Phys. Rev. Lett. 65, 964 (1990); Phys. Rev. D 46, 381 (1992).
- [62] W. Grimus, L. Lavoura, O. M. Ogreid, and P. Osland, J. Phys. G 35, 075001 (2008); Nucl. Phys. B 801, 81 (2008).
- [63] H. E. Haber and D. O’Neil, Phys. Rev. D 83, 055017 (2011).
- [64] R. M. Winters and D. O’Neil, (2010) <http://people.bridgewater.edu/~doneil/STellipseModule.nb>.
- [65] The ALEPH, DELPHI, L3, and OPAL Collaborations (the LEP Higgs Working Group), Report No. LHWG Note/2001-05, arXiv: hep-ex/0107031.
- [66] E. Cerveró and J.-M. Gérard, Phys. Lett. B 712, 255 (2012).
- [67] The Heavy Flavor Averaging Group, arXiv: 1412.7515; see also <http://www.slac.stanford.edu/xorg/hfag/>.
- [68] J. Yu, PoS (LATTICE 2013), 398 (2013).
- [69] A. Lenz, Reports No. IPPP/14/85 and No. DCPT/14/170, arXiv: 1409.6963.
- [70] A. Lenz and U. Nierste, Reports No. TTP11-03 and No. TUM-HEP-792/11, arXiv:1102.4274.
- [71] A. Lenz, U. Nierste, J. Charles, S. Descotes-Genon, A. Jantsch, C. Kaufhold, H. Lacker, S. Monteil, V. Niess, and S. T’Jampens, Phys. Rev. D 83, 036004 (2011).
- [72] S. Aoki et. al. (FLAG Working Group), Eur. Phys. J. C 74, 2890 (2014).
- [73] A. Hocker and Z. Ligeti, Annu. Rev. Nucl. Part. Sci. 56, 501 (2006).
- [74] J. Charles, S. Descotes-Genon, Z. Ligeti, S. Monteil, M. Papucci, and K. Trabelsi, Phys. Rev. D 89, 033016 (2014).
- [75] B. McWilliams and O. Shanker, Phys. Rev. D 22, 2853 (1980).
- [76] R. S. Gupta and J. D. Wells, Phys. Rev. D 81, 055012 (2010).
- [77] A. Lenz, U. Nierste, J. Charles, S. Descotes-Genon, H. Lacker, S. Monteil, V. Niess, and S. T’Jampens, Phys. Rev. D 86, 033008 (2012).
- [78] E. Golowich, J. A. Hewett, S. Pakvasa, and A. A. Petrov, Phys. Rev. D 76, 095009 (2007).
- [79] C. Q. Geng and J. N. Ng, Phys. Rev. D 38, 2857 (1988).
- [80] The ATLAS Collaboration, Report No. CERN-PH-EP-2015-229, arXiv: 1509.06047.
- [81] K. G. Chetyrkin, R. Harlander, T. Seidensticker, and M. Steinhauser, Phys. Rev. D 60, 114015 (1999).

- [82] The CMS Collaboration, JHEP 02, 024 (2014).
- [83] M. Czakon, P. Fiedler, and A. Mitov, Phys. Rev. Lett. 110, 252004 (2013).
- [84] The CMS Collaboration, Report No. CMS-PAS-SUS-13-013.
- [85] A. D. Martin, W. J. Stirling, R. S. Thorne, and G. Watt, Eur. Phys. J. C 63, 189 (2009); see also <http://mstwpdf.hepforge.org/>.
- [86] The CMS Collaboration, Reports No. CMS-HIG-14-005 and No. CERN-PH-EP-2015-027, arXiv: 1502.07400.
- [87] The ATLAS Collaboration, Report No. CERN-PH-EP-2015-184, arXiv: 1508.03372.
- [88] K. Hayasaka et. al. (Belle Collaboration), Phys. Lett. B 666, 16 (2008).
- [89] B. Aubert et. al. (BaBar Collaboration), Phys. Rev. Lett. 104, 021802 (2010).
- [90] J. Adam et. al. (MEG Collaboration), Phys. Rev. Lett. 110, 201801 (2013).
- [91] W. J. Marciano and A. I. Sanda, Phys. Lett. B 67, 303 (1977).
- [92] Y.-N. Mao and S.-H. Zhu, Phys. Rev. D 93, 035014 (2016), arXiv: 1505.07668.
- [93] S. Davidson and G. Grenier, Phys. Rev. D 81, 095016 (2010).
- [94] Y. Omura, E. Senaha, and K. Tobe, JHEP 05, 028 (2015).
- [95] Y. Omura, E. Senaha, and K. Tobe, arXiv: 1511.08880.
- [96] S. M. Barr and A. Zee, Phys. Rev. Lett. 65, 21 (1990); Phys. Rev. Lett. 65, 2920 (1990).
- [97] D. Chang, W.-S. Hou, and W.-Y. Keung, Phys. Rev. D 48, 217 (1993).
- [98] R. Harnik, J. Kopp, and J. Zupan, JHEP 03, 026 (2013).
- [99] G. 't Hooft, Phys. Rev. Lett. 37, 8 (1976); J. E. Kim and G. Garosi, Rev. Mod. Phys. 82, 557 (2010).
- [100] J. Brod, U. Haisch, and J. Zupan, JHEP 11, 180 (2013).
- [101] T. Abe, J. Hisano, T. Kitahara, and K. Tobioka, JHEP 01, 106 (2014).
- [102] K. Cheung, J. S. Lee, E. Senaha, and P.-Y. Tseng, JHEP 06, 149 (2014).
- [103] L. Bian, T. Liu, and J. Shu, Phys. Rev. Lett. 115, 021801 (2015).
- [104] A. Soni and R. M. Xu, Phys. Rev. Lett. 69, 33 (1992).
- [105] D. Atwood, S. Bar-Shalom, G. Eilam, and A. Soni, Phys. Rep. 347, 1 (2001).
- [106] S. Weinberg, Phys. Rev. Lett. 63, 2333 (1989); D. A. Dicus, Phys. Rev. D 41, 999 (1990).
- [107] E. Braaten, C.-S. Li, and T.-C. Yuan, Phys. Rev. Lett. 64, 1709 (1990).
- [108] The CMS Collaboration, Eur. Phys. J. C 73, 2604 (2013), arXiv: 1304.7498.
- [109] The CMS Collaboration, Phys. Rev. Lett. 111, 101804 (2013).

- [110] The LHCb Collaboration, Phys. Rev. Lett. 111, 101805 (2013).
- [111] The CMS and LHCb Collaborations, Nature 522, 68 (2015).
- [112] A. J. Buras, J. Girrbach, D. Guadagnoli, and G. Isidori, Eur. Phys. J. C 72, 2172 (2012).
- [113] C. Bobeth, M. Gorbahn, T. Hermann, M. Misiak, E. Stamou, and M. Steinhauser, Phys. Rev. Lett. 112, 101801 (2014); T. Hermann, M. Misiak, and M. Steinhauser, JHEP 1312, 097 (2013).
- [114] X.-Q. Li, J. Lu, and A. Pich, JHEP 06, 022 (2014), arXiv: 1404.5865.
- [115] M. Misiak et. al., Phys. Rev. Lett. 114, 221801 (2015); M. Czakon, P. Fiedler, T. Huber, M. Misiak, T. Schutzmeier, and M. Steinhauser, JHEP 1504, 168 (2015).
- [116] T. Hermann, M. Misiak, and M. Steinhauser, JHEP 1211, 036 (2012); see also the mathematica code <http://www.ttp.kit.edu/Progdata/ttp12/ttp12-29/>.
- [117] M. Casolino, T. Farooque, A. Juste, T. Liu, and M. Spannowsky, Eur. Phys. J. C 75, 498 (2015).
- [118] J. L. Abelleira Fernandez et. al. (LHeC Study Group), J. Phys. G 39, 075001 (2012), arXiv: 1206.2913.
- [119] E. Cruz-Alaniz, D. Newton, R. Tomás, and M. Korostelev, Phys. Rev. ST Accel.Beams 18, 111001 (2015).
- [120] Y.-L. Tang, C. Zhang, and S.-H. Zhu, arXiv: 1508.01095.
- [121] M. Bicer et. al. (The TLEP Design Study Working Group), JHEP 01, 164 (2014).
- [122] M. Aicheler et. al., Reports No. CERN-2012-007, No. SLAC-R-985, No. KEK-Report-2012-1, No. PSI-12-01, and No. JAI-2012-001.
- [123] M. Ahmad et. al. (The CEPC-SPPC Study Group), Reports No. IHEP-CEPC-DR-2015-01, IHEP-TH-2015-01, and IHEP-EP-2015-01, <http://cepc.ihep.ac.cn/preCDR/volume.html>, (2015) .
- [124] C. Adolphsen et. al., arXiv: 1306.6328; arXiv: 1306.6353.
- [125] The CMS Collaboration, Report No. CMS-PAS-FTR-13-024.
- [126] The LHC Higgs Cross Section Working Group, Report No. CERN-2011-002, arXiv: 1101.0593.
- [127] C. S. Huang and S.-H. Zhu, Phys. Rev. D 60, 075012 (1999); S.-H. Zhu, Phys. Rev. D 67, 075006 (2003).
- [128] K. Huitu, S. K. Rai, K. Rao, S. D. Rindani, and P. Sharma, JHEP 04, 026 (2011).

- [129] X. Gong, Z.-G. Si, S. Yang, and Y.-J. Zheng, Phys. Rev. D 87, 035014 (2013).
- [130] Q.-H. Cao, X. Wan, X.-P. Wang, and S.-H. Zhu, Phys. Rev. D 87, 055022 (2013).
- [131] D. Asner et al., arXiv: 1310.0763.
- [132] M. Battaglia, A. Ferrari, A. Kiiskinen, and T. Maki, eConf C010630, E3017 (2001), arXiv: hep-ex/0112015.
- [133] Y.-N. Mao, PhD Thesis (2016); G. Li, Y.-N. Mao, C. Zhang, and S.-H. Zhu, in preparation; G. Li, Y.-N. Mao, and S.-H. Zhu, in preparation.
- [134] The CMS Collaboration, Report No. CMS-NOTE-13-002, arXiv: 1307.7135.
- [135] The ATLAS Collaboration, Report No. ATL-PHYS-PUB-2013-007, arXiv: 1307.7292; Report No. ATL-PHYS-PUB-2013-014.
- [136] S. Berge, W. Bernreuther, and J. Ziethe, Phys. Rev. Lett. 100, 171605 (2008); S. Berge, W. Bernreuther, and S. Kirchner, Phys. Rev. D 92, 096012 (2015).
- [137] S. Berge, W. Bernreuther, and H. Spiesberger, Phys. Lett. B 727, 488 (2013).
- [138] P. S. Bhupal Dev, A. Djouadi, R. M. Godbole, M. M. Mühlleitner, and S. D. Rindani, Phys. Rev. Lett. 100, 051801 (2008); R. M. Godbole, C. Hangst, M. Mühlleitner, S. D. Rindani, and P. Sharma, Eur. Phys. J. C 71, 1681 (2011).
- [139] T. Aushev et. al., Report No. KEK Report 2009-12, arXiv: 1002.5012.
- [140] The SuperB Collaboration, Report No. INFN/AE-10/2, No. LAL-110, and No. SLAC-R-952, arXiv: 1008.1541.
- [141] S. Khatibi and M. M. Najafabadi, Phys. Rev. D 90, 074014 (2014).
- [142] The LHCb Collaboration, Reports No. CERN-LHCC-2011-001 and No. LHCC-I-018; Reports No. CERN-LHCC-2012-007 and No. LHCb-TDR-12.
- [143] The CMS Collaboration, Report No. CMS-PAS-FTR-13-022.
- [144] J. Kopp and M. Nardecchia, JHEP 1410, 156 (2014).
- [145] E. Levichev, Phys. Part. Nucl. Lett. 5, 554 (2008).
- [146] A. V. Bobrov and A. E. Bondar, Nucl. Phys. B (Proc. Suppl.) 225-227, 195 (2012); Nucl. Phys. B (Proc. Suppl.) 253-255, 199 (2014).
- [147] A. M. Baldini et. al. (MEG Collaboration), arXiv: 1301.7225.